NBSIR 78-1575

Erosion by Solid Particle Impact

A. W. Ruff and S. M. Wiederhorn

National Measurement Laboratory
Center for Materials Science
National Bureau of Standards

January 1979

Interim Report

Prepared for
The Office of Naval Research
Department of the Navy
Arlington, Virginia

DISCLAIMER NOTICE

THIS REPORT IS INCOMPLETE BUT IS THE BEST AVAILABLE COPY FURNISHED TO THE CENTER. THERE ARE MULTIPLE MISSING PAGES. ALL ATTEMPTS TO DATE TO OBTAIN THE MISSING PAGES HAVE BEEN UNSUCCESSFUL.

NBSIR 78-1575

EROSION BY SOLID PARTICLE IMPACT

A. W. Ruff and S. M. Wiederhorn

National Measurement Laboratory
Center for Materials Science
National Bureau of Standards

January 1979

Interim Report

Prepared for
The Office of Naval Research
Department of the Navy
Arlington, Virginia

U.S. DEPARTMENT OF COMMERCE, Juanita M. Kreps, *Secretary*

Jordan J. Baruch, *Assistant Secretary for Science and Technology*

NATIONAL BUREAU OF STANDARDS, Ernest Ambler, *Director*

Chapter 2 EROSION BY SOLID PARTICLE IMPACT

A. W. Ruff and S. M. Wiederhorn
Center for Materials Science
National Bureau of Standards
Washington, D.C. 20234

I Introduction

II Single Particle Erosion

A. Metals

1. Methods and Results
2. Interpretations

B. Ceramics

1. Results
2. Interpretations

III Multiple Particle Erosion

A. Metals

1. Methods and Results
2. Interpretations

B. Ceramics

1. Results
2. Interpretations

IV Theories of Erosion

A. Ductile Material Models

B. Brittle Material Models

C. Other Considerations

V Significant Parameters

A. Eroding Particle Characteristics

B. Eroded Material Characteristics

C. Environmental Effects

VI Summary and Recommendations for Future Work

VII References

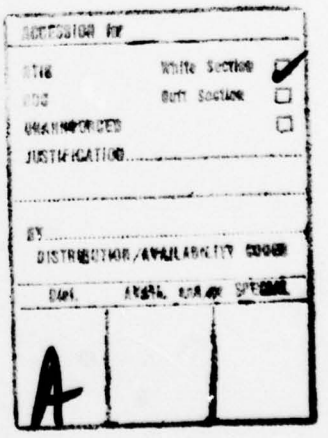

EROSION BY SOLID PARTICLE IMPACT

I. INTRODUCTION

The erosion of materials by surface impact of hard particles is one of several forms of material degradation generally classified as wear. It is by now well understood that wear is a complex phenomenon, consisting in fact of several simultaneous and interacting processes, typically involving mechanical, chemical and material parameters as well as complex mechanisms. This complexity in many instances seems to defy simplification on the part of the experimentalist seeking to carefully separate variables and the theorist attempting to accurately model the wearing system. However, in recent years considerable progress has been made both in gaining a basic appreciation of the significant parameters of wear and in applying a materials methodology to mitigate the problems of wear. While this Chapter will only address solid particle erosion, it is well to keep in mind that other wear processes, e.g., abrasive wear and oxidative wear, involve many similar characteristics and perhaps mechanisms. Progress in understanding any one of these processes may be applicable to others, and to the development of more wear resistant materials and systems.

Reviews of the state of information on solid particle erosion have appeared recently in several sources (Engel, 1976; Preece and MacMillan, 1977; Hutchings, 1978; Finnie et al, 1978). The state of earlier understanding has been adequately reviewed in several other articles (Finnie, 1960, 1972; Finnie et al, 1967; Ritter, 1963; Neilson and Gilchrist, 1968; Sheldon and Finnie, 1966, a, b); that information will not be repeated here. Rather we wish to

establish a framework for considering solid particle erosion, to review briefly only the central features of previous results, and to emphasize primarily the microstructural aspects of the problem. It is this latter area that appears to us to offer promise of further understanding of erosion (and wear) processes. Other chapters in this book will contain relevant information on microstructural and environmental effects and should be consulted for details. The mechanics of erosion, in particular, are addressed in detail in Chapter 1.

It has been very instructive we believe to examine the effects of solid particle erosion, first, on the basis of single particle impacts, and then under multiple impacting conditions. This chapter will review briefly recent work using that format, and then describe the theoretical situation. It is hoped that the reader can thereby appreciate what is known as well as what is yet needed. Significant parameter issues, e.g., surface temperatures and melting, strain rate effects, will then be described. Finally, our view of the needed future emphasis in this area will be described.

II. SINGLE PARTICLE EROSION

Erosive wear of materials in practice generally involves long times of exposure under steady state conditions. However, by its nature, solid particle erosion is a discrete, accumulative process and the single impact event is clearly worthy of as accurate an understanding as possible. It is also clear that multiple particle effects are to be expected; these will be treated later in the Chapter.

Single particle studies can be conducted over a wide size scale of particles, from millimeters to micrometers, through the use of quantitative measurement methods involving optical, scanning and transmission electron microscopes. Recent studies have produced extremely valuable information on the basic process of particle-surface impact.

A. METALS

1. Methods and Results

Two illustrations of eroded surface structures on a ductile metal are shown in Fig. 1. In one case discrete, isolated impact craters are seen (Fig. 1a), the result of a very brief exposure time. At longer exposure times, the more uniformly eroded surface shown in Fig. 1b results. Through considerable care in designing and using experimental apparatus, one can control the important parameters of particle orientation and velocity, and quantitatively investigate single particle erosion. Some recent studies are described below.

Various experimental techniques have been used to cause single particles to impact on specimen surfaces under controlled conditions. Electrostatic acceleration methods were employed by Shelton et al. (1960) and Hutchings and Winter (1974) in studies of small particle erosion effects. Explosive acceleration methods have also been reported (Hutchings and Winter, 1974), however most studies have used some type of gas-projectile gun. In this method, shown schematically in Fig. 2, a single projection of one or more erosive particles against the specimen surface is carried out. Large particles can be directly accelerated while micrometer sized particles are indirectly accelerated using a carrier or sabot (that does not strike or damage the specimen). Sheldon and Kanhere (1972) used this latter method to accelerate individual particles of silicon carbide, steel and glass shot about 3 mm in diameter at various velocities from about 130 m/s to 400 m/s. Both previously eroded and un-eroded surfaces were exposed and then studied. Erosion weight loss measurements also were made. Observations of the impact craters showed that the displaced crater material appeared to have flowed in the direction of particle

incidence until the material fractured at high accumulated strains. They noted considerable evidence of deformation adjacent to the crater in annealed material. In previously work-hardened specimens, the forward built-up edge seemed to fracture sooner.

Hutchings and Winter (1974) studied the erosion process using large (3mm) spherical particles; they placed particular emphasis on the geometry and mechanisms of metal removal. The characteristic deformation pattern resulting from particle impact consisted of a depression and a lip or rim of displaced material. Figure 3a shows the impact crater morphology found in this work for a steel sphere impacting on aluminum. A representation of the crater cross section is shown in Fig. 3b. They reported that smaller particles (down to 1 μm size) produced very similar patterns of deformation for the velocities studied (about 150 m/s to 200 m/s) on specimens of copper, mild steel and aluminum.

Studies of the erosion impact craters recently carried out using 50 μm Al_2O_3 particles have revealed similar structures (Ives and Ruff, 1978 a). Annealed AISI type 310 stainless steel specimens and copper specimens were impacted by spherical glass particles and also by angular Al_2O_3 particles at a velocity of 59 m/s. Two exposure angles of attack, 20° and 90°, were used in order to examine different modes of material removal. At the low angle, material was deformed and displaced from the crater into a lip at the exit end and sides. At 90° incidence, a more uniform lip of material around the crater was produced. There was considerable evidence of plastic flow within the impact crater region. Transmission electron microscopy (TEM) studies were carried out to investigate the sub-surface damage. Figure 4 shows an impact crater in

type 310 stainless steel produced by an irregular 50 μm Al_2O_3 particle that impacted at 90°angle and 59 m/s. The surface appearance (Fig. 4a) is consistent with the shape and size of the particles. The sub-surface damage, seen in Fig. 4b, was typical of that found at the craters. It consisted of a high density of dislocations formed in a well defined zone around the crater, extending a few micrometers in all directions. Some bands and groups of dislocations were observed but more usually a random tangle of dislocations around the crater walls was found. There was evidence of deformation twinning in some cases, and electron diffraction studies indicated polycrystalline regions, perhaps due to recrystallization. The dark central region in Fig. 4b results from strong electron scattering from the deformed material adjacent to the crater wall. Outside of the immediate crater region, the concentration of dislocations dropped sharply. Some slip plane arrays of dislocations were identified.

Plastic strain measurements were carried out using a selected area electron channeling method (Ruff, 1976) in order to further measure the erosion damage. This method which averages the strain over a volume of material of about 10 μm^3 showed that plastic strains greater than about 15% were associated with the impact craters in copper. The strains decreased rapidly with distance from the crater, and decreased with depth below the original surface as determined by electrolytic removal of material.

Studies carried out using 50 μm spherical glass particles (Ives and Ruff, 1978a) produced crater geometry and deformation patterns somewhat easier to analyze. The crater shown in Fig. 5a from a type 310 stainless steel specimen produced at an attack angle of 20° and velocity

2. Interpretations

Despite the few studies reported so far on single particle erosion, some essential features of the process have been identified. Particle shape and orientation at contact are clearly important parameters along with particle velocity, attack angle, and particle material properties. A difference in the characteristics of craters formed on uneroded and on previously eroded surfaces was found. Thus, single particle experiments alone are not sufficient. Sheldon and Kanhere (1972) also found a small difference in the velocity dependence of erosion between uneroded and previously eroded surfaces that is probably significant. These authors did observe that the displaced lip material appeared to detach earlier on previously eroded surfaces, reflecting apparently the higher strain levels in the material.

Hutchings and Winter (1973) found evidence for a critical particle velocity above which material is displaced from the crater lip. They suggested that frictional forces between the surface and the particle may be important in the crater formation process. Hence, the effect of environment (including surface films) on surface friction may need further consideration. These authors (Winter and Hutchings, 1974) also studied angular particle impacts where a micromachining process was identified. The details depended on particle rake angle and attack angle, as well on the extent to which particle fragmentation occurred. Figure 7 shows an interesting section through an impact crater in steel where both the configuration of displaced material and the pattern of deformation in the bulk material can be seen. Bands of local, intense shear were observed in some of the crater lips. Evidence for local heating leading to local

thermally affected deformation has been presented (Winter and Hutchings, 1975) and points up the need to consider thermal-mechanical properties of materials with regard to erosion behavior.

Transmission electron microscope studies of the damage associated with particle impact in copper and type 310 stainless steel (Ives and Ruff, 1978a) revealed a zone of high dislocation density typically a few micrometers thick around an impact crater. Strain measurements using the electron channeling method also showed a localization of damage near the craters. Deformation twins were formed at large angular particle craters, suggesting an intense local stress, possibly imposed at a high strain rate. Experiments using a diamond pyramid indentor to form impressions revealed similar dislocation patterns as were found near the impact craters, although deformation twins were not observed at the identations.

The recent results of Hutchings (1977a, 1978) clearly establish several modes of particle impact deformation. Particle shape was significant. Since angular particles either displace more material into the crater lip where it becomes vulnerable to further erosion or actually detach material from the surface (depending on particle rake angle at contact), the erosion efficiency of angular particles relative to round particles can be explained. In combination with these experiments, a theoretical model was developed to describe the particle interaction with the impacted surface. Calculations of the particle position and orientation with time were in good agreement with the experimental photographs of actual impact events. The limited range of rake angles, 0° to -17°, over which actual cutting was observed confirmed the calculations. It was pointed out that such impact conditions are infrequent, perhaps only occurring about once out of six impacts on a

random basis. Thus the crater lip formation process appears to be the dominant mode of impact damage, and loss of metal takes place primarily through subsequent impacts with the lip material. Recent observations on debris particles recovered from eroded 1015 steel surfaces support this picture (Ruff, 1978).

B. CERAMICS

1. Results

Erosion of ceramic materials has been generally viewed as a brittle process. This view is based on the observation that material removal occurs mainly by chipping. A more modern view of ceramic erosion is based on the assumption that plastic deformation plays a crucial role in the chipping process. In this section, the microscopic processes that occur during impact of brittle materials are described.

The morphology of fractures formed in ceramic materials during impact can be divided into two classes, depending on whether the impacting particle is blunt or sharp (Lawn and Wilshaw, 1975, Lawn and Marshall, 1978). Blunt particles, typified by spheres, result in the formation of cone-shaped cracks (Hertzian cracks), which initiate from pre-existing flaws that lie just outside the area of contact between the particle and the target surface (Fig. 8). The entire process of Hertzian crack formation is an elastic one that can be described by linear elastic fracture mechanics. Hertzian cracks form for a wide range of impact loads; however, as the contact forces increase above a level that is determined by the hardness of the material, plastic deformation occurs beneath the impacting particle, and a second set of cracks are observed to form normal to the impacted surface (Fig. 9, also see Evans and Wilshaw, 1976, 1977). This second set of cracks, termed radial, are more typical of the type that form as a result of sharp particle impact. Their formation suggests that the same plastic processes that govern crack formation for sharp particles become active when blunt particles impact at high loading levels. This point is clearly illustrated in the work of Evans and his colleagues (1978) who investigated the morphology of cracks formed by high velocity impact with solid particles. Thus, the distinction

between blunt and sharp particle impact is a distinction that depends on the role of plastic deformation in the impact process. The particle velocity that characterizes the transition between the formation of Hertzian cracks and the formation of radial cracks depends on the hardness, fracture toughness, and surface structure of the target material. In glass, for example, this transition occurs at ∿30 m/s for unabraded surfaces impacted with 0.8 mm radius steel or tungsten carbide spheres (Wiederhorn and Lawn, 1977). The transition occurs at lower velocities for pre-abraded glass surfaces.

Because Hertzian cracks initiate from pre-existing surface flaws, a minimum threshold stress (corresponding to a minimum impact velocity) is required for Hertzian crack formation (Evans, 1973, Wiederhorn and Lawn, 1977, Kirchner and Gruver, 1977). The threshold stress for crack formation is governed by the radius of the impacting particle, and the fracture resistance of the material (the critical stress intensity factor). The size of the flaw that initiates the Hertzian crack plays a secondary role in Hertzian crack formation (Lawn and Langitan, 1969).

Impact by sharp particles (angular rather than round) results in a distinctly different type of crack pattern in the target surface. Two types of cracks are observed: the first type is a radial set of cracks oriented primarily perpendicular to the target surface; the second type is a lateral set of cracks oriented primarily parallel to the target surface (Fig. 10). The radial set of cracks are primarily responsible for strength degradation, whereas the lateral set are responsible for erosive wear. As can be ascertained from static indentation tests (Lawn and Swain, 1975, Evans and Wilshaw, 1976), radial cracks form during the loading portion of the impact cycle, whereas lateral cracks form as the particle leaves the

target surface. Once radial cracks have initiated, the driving force for fracture is the wedging action of the impacting particle. By contrast, lateral cracks are formed as a result of residual plastic deformation at the point of contact. Lateral cracks usually curve and propagate to the target surface, resulting in chip formation and loss of material from the target surface.

The threshold velocity for crack formation is considerably lower for sharp particles than for blunt particles. For example, 30 mesh abrasive SiC particles ($\sim$0.6 mm sieve opening) dropped from a height of 1 cm (velocity $\sim$.4 m/s at contact) onto the surface of glass results in a significant decrease in strength due to crack formation (Wiederhorn and Lawn, 1979). By contrast, velocities of $\sim$30 m/s are required for Hertzian crack formation caused by 0.4 mm diameter tungsten carbide spheres (Wiederhorn and Lawn, 1977). Theoretical estimates of the load for radial crack formation have been presented by Lawn and Evans (1977) using an elastic-plastic analysis. They indicate that the critical load depends on both the hardness and the critical stress intensity factor of the target material.

Direct evidence for plastic flow during impact has been obtained from transmission electron microscope studies of surfaces that have been impacted with hard particles (Hockey et al., 1978). These studies were conducted on a group of brittle crystalline materials with very different properties. Microstructural features were very similar to those observed in static indentation studies (Hockey, 1971, Hockey and Lawn, 1975). Dense tangles of dislocations were observed at the impact site for all materials; the density of dislocations was similar to that observed in metals. The dislocation and crack morphology in ceramics depended on the crystal structure. For MgO (Fig. 11), dislocation arrays propagated on (110) planes well beyond the impact area, a behavior that is consistent with the ease of deformation

of ionic crystals on (110) planes. Cracks also propagated on (110) planes in this crystal, but were contained within the dislocation arrays. Silicon and germanium, which are covalent, also exhibited dense arrays of dislocations at the contact site, but now the dislocations were tightly bound to the immediate vicinity of the contact site (Fig. 12). Cracks that were generated during impact propagated well beyond the immediate contact site often resulting in extensive surface chipping. Materials that possess partial covalent and partial ionic behavior (Al_2O_3, SiC) exhibited a somewhat intermediate behavior during impact (Fig. 13). Both dislocations and cracks propagated well beyond the contact area during impact.

Temperature has the effect of increasing dislocation mobility in crystalline materials, so that a material dependent critical temperature should exist for transition from elastic-plastic to plastic impact conditions. In an attempt to investigate temperature effects on erosion, Hockey et al., (1978) exposed Al_2O_3 crystals to erosive particles at 1000°C. Optical microscopy investigations of the target surface revealed little change in the erosion crack morphology: material removal from the Al_2O_3 surface at 1000°C was still primarily by chipping (Fig. 14). Consistent with this observation is the fact that temperature had little effect on bulk erosion rates of Al_2O_3 (Hockey et al., 1978). Transmission electron microscopy observations, however, did reveal a considerable increase in the relative extent of the deformation associated with impact at high temperatures. In contrast to room temperature results, the radial extent of deformation by slip at 1000°C was found to be comparable to the extent of fracture. In

addition, impact at 1000°C resulted in a significant increase in the amount of twinning over that occurring at room temperature. High temperature impact resulted in numerous interactions between slip bands, twins, and grain boundaries outside of the immediate area of contact. Nevertheless, this deformation was not sufficient to prevent chipping at the impact site. Apparently, temperatures greater than 1000°C are needed to obtain completely ductile erosion for a material such as Al_2O_3.

The amount of cracking of ceramic materials during impact can be modified significantly by reducing the angle of impact (Hockey et al., 1978). At 15° impact, cracking on ceramics is largely eliminated. The cracking that is observed is primarily of the lateral type. Shallow residual impressions in the ceramic surface are observed (Fig. 15). These are elongated in the direction of particle motion (in the same way as for metals) suggesting a shear deformation mechanism of erosion at low impact angles. Indeed, examination of the contact area by transmission electron microscopy (Fig. 16) confirms the absence of cracks and the predominance of plastic deformation in the contact area. Thus at low impact angles, ceramic materials appear to erode by plastic deformation; in this regard their behavior is similar to that found in metals.

2. Interpretation

From the above discussion it is clear that a deeper understanding of single particle impact in ceramics requires a distinction to be made between completely elastic impact events and elastic-plastic impact events. In this section, theories of crack formation during impact are reviewed. In succeeding sections the results of these theories are used to develop models that predict rates of erosion during multiple particle impact.

As mentioned above, impact with blunt particles requires a minimum threshold velocity for crack formation. Evans (1973), and Wiederhorn and Lawn (1977) used linear elastic fracture mechanics to describe the size of the Hertzian crack formed during impact. A quasi-static approximation is used to convert impact velocity to maximum impact force. The kinetic energy is assumed to be completely converted into elastic energy during impact. The maximum impact force is then calculated from the stored elastic energy at deepest penetration of the particle into the target surface. The maximum impulse load, F_m, depends on the elastic constants of the target material and particle, and on the density, ρ, radius, r, and velocity, v_o, of the particle:

$$F_m = [(125\ \pi^3/48)^{1/5}\ (E/k)^{2/5}\ \rho^{3/5} r^2]\ v_o^{6/5} \qquad (1)$$

E is Young's modulus of the target and $k = 9/16[(1-\nu^2)+(1-\nu'^2)(E/E')]$ is a dimensionless quantity that depends on Poisson's ratio, ν of the target, and ν' of the particle, and on Youngs modulus, E of the target, and E' of the particle.

The critical load, F, for crack growth during impact is determined from the size of the critical flaw in the target surface. For the case of quasi-static impact, Lawn and Wilshaw (1975), and Frank and Lawn (1967) developed the requisite fracture mechanics equations for crack growth. Because Hertzian stress fields are not homogeneous, a single, simple analytical expression cannot be derived for the critical load as a function of flaw size. It is, however, possible to show that simple limit expressions can be given for very small flaws ($c_f^\circ << 0.01a$), and for large flaws ($c_f^\circ \gtrsim 0.01a$), where a is the contact radius between the sphere and the surface at maximum penetration. For most practical situations, the critical load, F, is given by the large flaw approximation,

for which Auerbach's law (1891) is valid (Lawn and Marshall, 1978); $F = Ar$, where A is a constant that is determined by the critical stress intensity factor, K_c, of the target material ($A = K_c^2 k/E\phi^*$; ϕ^* is a dimensionless, material constant whose values are obtained experimentally). By substituting F_m into Auerbach's law, the critical velocity, v_c, is obtained for Hertzian crack formation (Wiederhorn and Lawn, 1977)

$$v_c = (48/125\pi^3)^{1/6} (k/E)^{7/6} K_c^{5/3}/\rho^{1/2} r^{5/6} \phi^{*5/6}. \quad (2)$$

For particle velocities less than this critical velocity, fracture, and hence erosion, will not occur. Above v_c, the crack size is determined by a second equation that was derived by Roesler (1956), who used a Griffith type energy balance in combination with a dimensional analysis:

$$F/R^{3/2} = \beta_R K_c . \quad (3)$$

F is the impulse load, R is the base radius of the cone crack formed during impact, and β_R is a constant that is usually determined empirically. Substituting equation (1) into equation (3) (i.e. $F = F_m$), the following equation is obtained for the size of the cone crack that forms as a result of impact:

$$R = [(125\pi^3/48)^{2/15} (E/k)^{4/15} \rho^{2/5} r^{4/3}/\beta_R^{2/3} K_c^{2/3}] v_o^{4/5}. \quad (4)$$

The cone crack radius, R, can be used to estimate strength degradation resulting from impact. Assuming the effective flaw size for fracture, c_f, is proportional to R, $c_f = \Omega R$, then strength degradation is determined by substituting Eq. (4) into the Griffith equation, $\sigma = K_c/(\pi c_f)^{1/2}$:

$$\sigma = [(48/125\ \pi^{10.5})^{1/15} (k/E)^{2/15} \beta_R^{1/3} K_c^{4/3}/\Omega^{1/2} \rho^{1/5} r^{2/3}] v_o^{-2/5}. \quad (5)$$

The validity of this approach to Hertzian crack formation has been checked recently on several ceramic materials. Wiederhorn and Lawn (1977) have shown that the theory predicts the effect of particle velocity,

particle density, and particle size on the strength of glass impacted by steel and tungsten carbide spheres. Evans (1973) has shown that strength data obtained by Ashford (1968) on SiC is explained by the above theory. Although Kirchner and Gruver (1977) also obtained reasonable predictions of strength degradation of glass impacted with glass spheres, they never-the-less found that the crack size formed during impact was significantly less than that calculated from theory. From these results it can be concluded that the theory for predicting crack formation in the elastic impact situation is generally supported by experimental data. Clearly, additional work is needed to fully evaluate the theory, which does not completely account for the shape of the cracks formed on impact. Loading history appears to play some role in determining the crack shape, as evidenced by small rims that are observed to form along the edge of the Hertzian cracks as the particle leaves the surface (Chandhri and Walley, 1978). The formation of these rims may be the result of elastic wave generation during crack formation, residual plasticity at the impact site, or rebound of the surface as the sphere leaves the target. Despite some differences between experiment and theory, the theory does explain most major observations of spherical particle impact.

Sharp particle impact theories require a greater number of assumptions than blunt particle impact theories because plastic deformation occurs during impact. As noted by Lawn and Evans (1977) in their model for crack initiation in elastic-plastic indentation fields, crack initiation is determined by the stresses set up by the plastic zone that forms on impact. Their model can be applied to explain crack initiation for the case of quasi-static impact. Pre-existing flaws at the impact site are assumed to be the sources of crack formation. These

flaws grow as a result of the plastic stress field formed during impact. The hardness, H, and the contact radius (or an equivalent parameter), a, are convenient scaling parameters used to establish the stress in the vicinity of the flaw. Applying fracture mechanics theory, Lawn and Evans derive a critical crack size, c^*, and a critical load, F^*, for fracture, both of which depend on the hardness and critical stress intensity factor of the target material:

$$c^* = (1.767/\Theta^2)\ (K_c/H)^2 \tag{6}$$

$$F^* = (54.57\ \alpha/\eta^2\Theta^4)\ (K_c/H)^3 K_c\ . \tag{7}$$

α is a constant that depends on the indenter geometry ($\alpha = 2/\pi$ for a Vickers diamond pyramid indenter); Θ is a dimensionless constant that relates hardness to the maximum stress beneath an indenter; η is another dimensionless constant that relates the depth of the maximum stress to the size of the hardness impression. From equation 6 we note that unless a critical flaw larger than c^* is located in the vicinity of the indenter, fracture will not occur during indentation. The critical load for fracture, F^*, calculated by Lawn and Evans (1977) is shown to vary for a variety of materials, from 0.003 N (silicon) to 40 N (NaCl). The value obtained for glass, $F^* = 0.02$N, is considerably less than that obtained for any practical sphere size. A 0.4 mm radius sphere, for example, requires a load of 98.5 N to form a crack, whereas a sphere of approximately 0.1 μm would be required to generate a crack under a load of $\sim$0.02 N.† Thus, the theory by Lawn and Evans demonstrates the greater sensitivity of ceramic materials to sharp particle erosion than to blunt particle erosion.

Assuming a crack can be generated during impact, it is necessary to develop a mechanism of load transfer from the particle to the target

† Spheres of this radius are, of course, "sharp" from a microscopic point of view.

surface in order to estimate the final crack size resulting from the impact. The problem of load transfer arises because a complete elastic-plastic solution of the indentation process is not available. Hence the rate of particle deceleration, and consequently, the change in particle momentum at the target surface is not known. Two models have been proposed to estimate the contact force during impact. In one (Wiederhorn and Lawn, 1979), the kinetic energy of the particle is assumed to be completely dissipated by plastic flow as the particle contacts the surface. The contact force is calculated from the hardness of the target material and the maximum depth of penetration during contact. The maximum load, F_m, during contact is determined by the mass, m, of the particle, the hardness, H, of the target, the particle velocity, v_o, and several geometric constants that are governed by particle shape:

$$F_m \propto H^{1/3} m^{2/3} v^{4/3} \tag{8}$$

The size of the crack formed during impact is then determined by substituting Eq. (8) into Eq. (3)*, which is tantamount to assuming that a crack formed during impact depends on the load in the same way as one formed during static indentation:

$$c_f \propto m^{4/9} H^{2/9} v^{8/9} K_c^{-2/3}. \tag{9}$$

Evans, Gulden, and Rosenblatt (1978) included dynamic effects in their calculation of the contact force during impact. In contrast to the assumptions made by Wiederhorn and Lawn (1979), plasticity as represented by the hardenss is assumed to play a minor role in the fracture process. A spherical particle is assumed to penetrate into the target surface without distortion, and the contact pressure is assumed to be the dynamic pressure set up when the particle first hits the surface. The depth of penetration is determined from the time of contact, and the mean interface velocity, both of which are calculated from a one dimensional

*Eq. (3) has been shown by Lawn and Fuller (1975) to be valid for the formation of radial cracks in brittle materials.

impact analogue. The final expression obtained by Evans et al., (1978) for the contact force is considerably different from that obtained by Wiederhorn and Lawn:

$$F_m \propto v^2 R^2 \rho \tag{10}$$

Here R is the particle radius and ρ is its density. The size of the crack formed during impact is obtained by substituting Eq. (10) into Eq. (3)*:

$$c_r \propto [(v\ r)^2/K_c]^{2/3}\ \rho^{2/3}. \tag{11}$$

By comparing Eq. (11) with Eq. (9) we see that the two theories result in different expressions for radial crack formation. However, both expressions suggest that crack formation depends on $K_c^{-2/3}$. The theory by Evans et al. suggests a stronger dependence of crack size on velocity ($v^{4/3}$) than does the theory by Wiederhorn and Lawn ($v^{8/9}$). Furthermore, the theory by Wiederhorn and Lawn takes into account the hardness of the target material, whereas the theory by Evans et al. does not. Evans et al. compared their theory with data giving crack size as a function of particle velocity, particle shape and size, and target properties. In all cases good agreement was obtained between theory and experiment. In a more limited but similar set of experiments on glass, Wiederhorn and Lawn also obtained good agreement between theory and experiment. Additional experimental data and a detailed comparison of the two theories with the data will be needed to decide which of them better describes the impact process in terms of particle/target parameters.

*In comparing Eq. (11) with experimental data, Evans et al. (1978) discovered a weak dependence of c_r on ρ. Consequently, Evans et al. deleted ρ from Eq. (11) for further theoretical analysis. However since ρ enters the theory again in estimating the erosion rate, it was felt best to use Eq. (11) as it appears above. As a consequence the erosion rate (Eq. (20)) based on the above theory differs from that published by Evans et al.

Evans, Gulden and Rosenblatt (1978) also developed a theoretical description of lateral crack formation. The theory takes into account both the depth at which the lateral cracks form and the size to which they propagate. The depth, h, at which lateral cracks form is assumed to be proportional to the plastic zone depth at full penetration of the impacting particles. The problem of estimating the penetration depth had been addressed for a variety of impact conditions by Goodier (1965). Using Goodier's results and experimental data on depth of crack formation, Evans et al., (1978) relate the depth of crack formation, h, to the particle size, r, particle velocity, v_o, particle density, ρ, and target hardness, H:

$$(h/r)^2 \propto v_o(\rho/H)^{1/2} \tag{12}$$

The size of lateral cracks formed during impact is found experimentally to be proportional to the size of the radial cracks formed during impact. Thus, the semi-empirical model proposed by Evans et al., (1978) provides a quantitative description of lateral crack formation during impact.

III. MULTIPLE PARTICLE EROSION

Technological concern with the erosion of materials involves multiple particle impacts, usually in a steady state long term regime (National Research Council, 1977). Simple consideration of the effects of a flux of particles incident on a surface for some length of time suggests that many new, complex aspects are added to the basic problem. These include particle impacts within the incident stream, a wide range of simultaneous attack angles, particle fragmentation, surface shielding due to rebounding particles, and particle embedding effects among others. (Some of these effects, e.g., fragmentation and embedding also occur on single particle impact). Clearly multiple particle erosion exposures must be conducted in order to measure meaningful erosion rates of materials for application purposes. A second reason for such experiments would involve a search for new, significant effects due to multiple particles. One such effect has recently emerged concerning particle embedding in the specimen surface. Another important effect is that of subsurface damage due to multiple impacts. This section will review principally the recent work in this area.

A. METALS

1. Methods and Results

Two basic types of equipment design have been used to expose solid specimens to a stream of erosive particles. In one design the specimen is moved at a controllable velocity, usually on a rotating arm fixture, through a slowly moving erosive stream. The exposure may be intermittent but can continue for a long time period. The relative particle-specimen velocity can be accurately determined since the principal velocity component is that of the specimen (in the laboratory system). A variation on this design allows the erosive particles to be spun from a rotating disk to strike a fixed specimen. The alternative design involves propelling a stream of particles at a fixed specimen. The specimen may be completely immersed in the stream, or perhaps only a portion of the specimen exposed. In this scheme some method of measuring or calculating particle velocity must be used. The particle concentration in the stream and the nature of the carrier gas (fluid) can be chosen as appropriate. Some type of nozzle or flight tube is involved in order to properly confine the erosive stream. Velocities of 300 m/s and larger have been reported using this method (for example, Grant and Tabakoff, 1975).

Quantitative measurements of erosion rate require careful attention to the experimental system and the parameters of exposure. For example, wear of the abrasive delivery nozzle can greatly alter the stream shape and velocity profile. Turbulance within a flight tube or caused by the presence of the specimen itself in the stream can significantly affect particle flux and particle velocity as experienced by the test specimen. Consideration of the particle trajectories within the incident stream, particularly near the specimen, are important (Tilly, 1969). Since, as we shall see, the erosion rate can vary as high as the third power of the particle velocity, accurate knowledge of

particle impact velocity is essential.

The variation of erosion, usually measured in mass or volume loss from the specimen per unit mass of impacting abrasive, as a function of angle of attack of the particles is shown schematically in Fig. 17 for brittle and for ductile materials. Many workers have reported this general behavior. For ductile materials the peak erosion loss occurs at around 20°. For brittle materials the peak erosion loss occurs at around 90° (normal incidence). The dependence of erosion rate on particle velocity has been measured for many materials over at least three orders of magnitude in velocity. The erosion rate is found to increase as v^2 to v^3 in most cases (see for example, Sheldon and Kanhere, 1972; Finnie et al, 1967). The velocity exponent has been reported not to depend on the type of material (Fig. 18), however, detailed studies have shown some dependence of the velocity exponent on attack angle (Fig. 19) and a dependence on the temperature of erosion (Fig. 20).

The dependence of erosion on particle size has also been studied by several workers. In a detailed study, Goodwin et al, (1969) examined the erosion of steel by quartz particles over a large size range. As shown in Fig. 21, an increase in erosion with increasing particle size was found up to a limiting size, above which the erosion remained constant.* A theory explaining this result has been developed (Tilly, 1973) and will be discussed later. Much interest has been centered on the possible erosion effects of very small particles e.g., less than 5μm in diameter. There have been conflicting reports in the literature on the size effect for such small particles. Recent studies have shown significant erosion of metals by particles as small as 2μm (Goebel et al, 1976).

---

*An increase in erosion was noted for particle sizes greater than about 500μm.

The effect of particle size as measured using flat test specimens may not be applicable in all geometries as shown by the recent work of Mills and Mason (1977). In studying erosion in 90° tube bends due to the conveying of abrasive sands, they reported that depth of penetration for 70 μm particles was much greater than for 230 μm particles. Further a different surface morphology resulted and a different angle of maximum penetration was found.

The effects of increasing temperature on erosion have been studied in more detail in the last few years. The environment in which high temperature erosion takes place usually has a very significant effect on erosion rate but will not be considered here (see, however, Chapter 8 for this question). Depending on the material being eroded, the temperature range, and the environment, different effects due to temperature have been reported (Young and Ruff, 1976). The results in one specific instance shown in Fig. 20 reveal a large increase in erosion of type 310 stainless steel on going from 25°C to 975°C. A recent study of erosion of aluminum and type 310 stainless steel (Finnie et al., 1978) also reported increased erosion for increased temperature, although a complicated dependence on erosion angle was reported (Fig. 22). In work on other alloys, however (Smeltzer et al., 1970), decreases in erosion with increasing temperature have been reported.

One material parameter that has been of particular interest in connection with the understanding of ductile material erosion is indentation hardness. Numerous correlation studies have been attempted to determine the relation of hardness to erosion rate. In Fig. 23 some results due to Finnie et al., (1967) are shown. Clearly the erosion rate of different ductile metals decreases as the reciprocal of material hardness. However, when those authors studied the effect of hardness variation for one alloy (varied through thermal treatments of a tool steel) they found little effect on erosion rate. Other differences between the materials studied such as the

crystal structure, slip systems, flow stress, and strain rate sensitivity, appear to be the determining parameters. Sheldon (1977) has recently proposed that the indentation hardness of a work-hardened surface would be a more appropriate measure to utilize.

The influence of other erosion parameters such as particle concentration in the erosive stream, particle hardness, and particle strength, have only been examined in a few instances. In the case of particle concentration, divergent findings have been reported as summarized by Uuemois and Kleis (1975). It would seem that relative erosion (specimen mass loss divided by impacting erosive mass) should be independent of particle concentration so long as each particle event is equally effective. At higher concentrations, where particle interference (shielding) effects occur at the specimen surface, the relative erosion should be expected to decrease and this has been reported (Uuemois and Kleis, 1975; Young and Ruff, 1977). Only limited studies of the effects of particle hardness, strength, and frangibility on the erosion of a given particle material have been reported (Tilly, 1973; Uuemois and Kleis, 1975). The interpretation of those results is complicated by the need for more extensive characterization of the particles before and after erosion. Recently, Maji and Sheldon (1978) have studied the effects of different mechanical conditions of spherical steel shot that were used as erosive particles. They examined the erosion of aluminum alloy tubes and flat plates using 270μm shot and found considerably more erosion for brittle than for ductile shot. Evidence for the removal of additional specimen material upon the fracture of an incident particle, so-called secondary erosion, was presented. At elevated temperatures, the hot hardness and high temperature toughness of both the specimen and the eroding

materials would be important to consider.

There has been attention given recently to the effect of particle embedding during erosion. Further, the effects of specimen microstructure on erosion behavior has been examined. Ives and Ruff (1978) have studied surface and subsurface erosion damage in copper exposed at room temperature and found evidence for significant particle embedding. As seen in Fig. 24, the initial erosion effect involves a mass gain of the specimen due to the added particulate matter. This results in an initial "incubation" period before the usual steady state erosion rate develops; this effect has been reported previously (Neilson and Gilchrist, 1968). Studies of the eroded copper specimens selected after various periods of exposure revealed a layer of deformed copper and abrasive (Al_2O_3) fragments that had developed at the surface, as seen in Fig. 25 . In these experiments an electrodeposit of copper was used to preserve the true surface structure during the preparation of cross-sections. Transmission electron microscopy studies of the effects of particle embedding were also reported; a region around one such particle is shown in Fig. 26 . Embedding was more pronounced at a 90° attack angle than at 20°, the other angle studied. A recent study by Zahavi et al. (1978) has also emphasized the occurrance of particle embedding during erosion studies of three different ductile alloys by natural sand particles.

It is possible to recover eroded material (metal and abrasive particles) after appropriately designed experiments. Preliminary studies have been carried out using mild steel (type 1015) specimens eroded at room temperature at 30° angle of attack using 50 μm Al_2O_3 particles (Ruff, 1978). Magnetic recovery methods were applied in this case to collect the metallic debris. Examples of recovered debris are shown in Fig. 27 where the aggregation of

individual particles is due to the impressed magnetic field used in recovery. The eroded surface structure is also shown. The majority of eroded metal particles are equiaxed and average about 3 μm in size. Many small metal particles were found less than 1 μm in size. Very few examples of particles of "cutting-like" morphology (ribbon or wire-like appearance) were found. A significant proportion of particles having a plate-like shape were seen. A good correspondence could be achieved between the observed metallic debris morphology and certain features of the metal surface topography. It appears that the metal debris was removed primarily from the exposed portions of surface impact crater features that were formed from plastic deformation associated with particle impacts. From the debris size and shape it does not appear that the metal debris particles were formed in a single cutting process but perhaps after several successive impact events. Examples were also found of abrasive particle fragments within the metallic debris clusters indicating transferred or adherent metal layers on the abrasive. Further studies of recovered metal and abrasive debris are in progress.

2. Interpretations

Review of the literature of erosion testing indicates many different methods and apparatus that have been used with considerable success. Frequently, multiple particle equipment is designed with some potential application geometry in mind. Perhaps a quantitative inter-comparison between different testing systems* would reveal some advantageous design in terms of the ability to reproduce the more critical parameters from test to test, but such information is not presently available. It is acknowledged that considerable care must be taken in accurately measuring the many parameters of erosion testing. Two critical experimental quantities can be mentioned here, particle velocity and particle attack angle. Several particle velocity measurement methods have been reported; photographic (Finnie et al., 1967), rotating disk (Ruff and Ives, 1975) and laser doppler (Goebel and Pettit, 1976). Particle velocity calculations have also been used in place of detailed measurements in some studies. The particle attack angle can ordinarily be measured accurately, however, for small particles (< 10 μm) flow pattern disturbances can produce large deviations from the nominal attack angle and must be considered. Such deviations near the peak erosion angle for ductile materials can lead to significant errors. Particle divergence within a stream and the effect of fragmentation on impact must also be considered carefully.

Results of multiple particle erosion studies on various materials have shown the effect of the principal parameters involved. Existing theoretical

---

*An inter-laboratory comparative measurement series involving solid particle erosion is presently beginning within the ASTM Committee G2 on Erosion and Wear.

models and calculations that consider these results will be described in the next section. The peak erosion angle of about 20° for ductile materials is ascribed to ploughing and cutting deformation processes with consideration also of particle fragmentation on impact. Brittle material erosion peaks at 90° incidence are related to the efficiency of crack formation around the impact crater. The particle velocity dependence of erosion, variously measured as proportional to v^2 to v^3 is still the subject of detailed investigation. In ductile materials the specific manner of deformation and cutting may determine the precise exponent value. Recent theoretical results of Hutchings (1978) and Finnie and McFadden (1978) address this matter.

The effects of particle size on erosion rate also need further study. For example, relatively little effort has been made to study particle size distributions before and after erosion and to characterize the erosion debris. Particle fracture and fragmentation phenomena have been reported; however, the importance of such issues is not agreed upon. Recently, Hutchings (1977) has proposed that the particle size effect (Fig.21) is due to the variation in imposed strain rate on impact with particle size.

The role of embedded particles (or fragments) on steady state erosion also needs more study. It appears that a layer of deformed metal and embedded particles forms as a result of the erosion of ductile material (Ives and Ruff, 1978). The sizes of the embedded particles are generally much smaller than the incident particles, as a result of fragmentation upon collision at the specimen surface. The mechanical properties of this mixed material surface layer and of the underlying material then determine the overall erosion behavior. Characterization of the subsurface damage produced during erosion below this mixed layer is also needed. It seems

possible that in some systems a degree of protection may even result from the embedding or adhesion of incident material in this manner.

The detailed deformation and fracture processes that take place as a result of particle impact on metals are not yet adequately understood. It appears from limited studies of erosion debris (Ruff, 1978) that, even at low (30°) attack angles, little metal may be removed by direct cutting impacts. Rather, plowing-type interactions producing extensive plastic deformation and displaced material create a surface topography (Fig. 27a) from which metal may be removed by subsequent particle impacts. In view of the complex topography of eroded surfaces it will be necessary to further examine the theoretical models that presently describe the erosion process.

Recent studies of erosion microstructures in metals by Levy and coworkers (Levy, 1978) have also shown some interesting subsurface structures resulting from deformation processes. Erosion of an aluminum alloy specimen using spherical particles produced a surface structure comprised of rounded hills of rippled appearance. A deformed surface layer of material was found that appeared to detach from the surface by a delamination type of process. Studies of this mechanism are reportedly continuing.

B. CERAMICS

1. Results:

The main parameter that controls the rate of erosion of materials is the particle velocity. A number of studies indicate that the erosion rate can be expressed as a power function of the particle velocity. As with metals (Finnie et al., 1967, Sheldon and Kanhere, 1977), velocity exponents generally range from ∿2 to ∿3 (Hockey et al., 1978, Sheldon 1970). Higher exponents have, however, been reported: 6 for glass impacted with steel spheres (Finnie, 1960); 4 for MgF_2 impacted with quartz, or silicon carbide (Gulden, 1978); 4 for silicon nitride impacted with quartz, or silicon carbide (Gulden, 1978). The value obtained for the velocity exponent of a given material apparently bears little relation to composition or microstructure of that material. Thus, castable refractories, which are ∿30 percent porous and have a multiphase structure, exhibit the same range of velocity exponents (2.3 to 3.9, Wiederhorn et al, 1977) as dense, relatively homogeneous ceramics such as glass, hot-pressed silicon nitride, and high density aluminum oxide (Hockey et al., 1978). In dense ceramic materials, grain size also has little apparent effect on the velocity exponent, even though it has a significant influence on the absolute rate of erosion. This insensitivity to composition and structure means that the velocity exponent is not a useful indicator for evaluating microstructural effects on erosion, or distinguishing between mechanisms of erosion.

Studies on both ceramics and metals suggest that impingement angle is a more satisfactory indicator of erosion mechanism. As noted earlier in this chapter, ductile materials (metals) exhibit a maximum in the erosion rate at an angle of impingement of approximately 20° (Fig. 17). By contrast, brittle materials (ceramics) exhibit a maximum in the

erosion rate at an angle of 90°. This type of behavior has been used to classify materials as either brittle or ductile with regard to erosion (Bitter, 1963, Neilson and Gilchrist, 1968, Sheldon 1970). Actually, most materials exhibit behavior that is neither completely ductile nor completely brittle, and quantitative procedures have been developed to evaluate the relative amounts of brittle and ductile erosion that occurs for a given material-particle system. Recent studies on ceramic materials indicate a strong contribution of ductile behavior in these primarily brittle materials.

Sheldon and Finnie (1966 a) were the first to demonstrate a ductile-to-brittle transition in ceramic materials. They showed that at a fixed velocity (∿150 m/s) the erosion behavior depended on the size of the impacting particle. Studies on glass, high-density magnesium oxide, and graphite indicated brittle type of erosion behavior for 127μm silicon carbide particles, whereas a change to a more ductile type of behavior was observed when the particle size was reduced to 9μm. This change in behavior was quite dramatic for glass, which exhibited a strong maximum in the erosion rate at an impact angle of ∿25°, as illustrated in Fig. 28. Moreover, microscopic studies of the eroded surfaces showed that the 127μm particles produced a chipped surface topography, wherease 9μm particles produced a ripple pattern, typical of ductile erosion, (Fig. 29). High density aluminum oxide, on the other hand, exhibited brittle erosion behavior for all particle sizes. These results indicate a significant effect of target material properties, even among materials that generally behave mechanically in a brittle fashion.

In a more recent discussion of the erosion behavior of materials, Sheldon (1970) noted the importance of tangential forces in the wear

process. For normal impact the erosion of brittle materials is proportional to v_o^b, where v_o is the particle velocity and b is the power exponent. If only brittle behavior were occurring at an oblique impact angle, then the erosion rate, w, might be expected to be proportional to $(v_o \sin \alpha)^b$, where α is the impact angle. By plotting ln w as a function of ln (sin α), Sheldon determined that, although the data fit straight lines, the power function b was not the same as that determined from velocity studies using normal impact angles. He concluded from these results that tangential forces contribute to the wear of brittle materials.

In a study of the effect of temperature on erosion, Hockey et al., (1978) also demonstrated that plastic flow processes occur during the erosion of brittle materials. The erosion rate of glass, silicon nitride, and aluminum oxide was measured as a function of temperature and impingement angle using ∿150μm silicon carbide particles as the erosion agent. Although a low angle maximum in the erosion rate was not observed in these studies, there did seem to be a significant enhancement of the erosion rate at low angles of impingement, Fig. 30. These findings were consistent with those reported earlier by Sheldon (1970). It was concluded that wear generally occurs by a mixed mode of erosion, with the ductile processes becoming increasingly more important with decreasing angle of impingement.

The above conclusions on ductile behavior are also supported by optical and scanning microscopy studies of erosion surfaces. Ceramic materials eroded at an impingement angle of 90° exhibit a rough, chipped surface indicative of material removal by a fracture process (Fig. 31). By contrast, erosive wear at 15° results in relatively smooth surfaces that are characterized by furrows, or wear scars, which indicate material

removal by a plowing mechanism, Fig. 32. Lateral cracks form at the margins of the wear scars, undoubtedly contributing to the wear process. This evidence for ductile erosion is consistent with single particle impact experiments (described above), which show extensive deformation in the impact area and a significant decrease in the incidence of fracture for low angles of particle impingement.

2. Interpretation

The results presented in the previous section point to the importance of plastic deformation in the erosion process. Subsurface plastic deformation at the impact site results in residual stresses that cause lateral crack formation and surface chipping, so that erosion appears to occur primarily by a brittle fracture process. The role of plastic deformation, relative to fracture, is enhanced by reducing the impact load during erosion. This can be accomplished by reducing the impact velocity, the particle size, or the angle of impingement. When the impact load falls below a critical value, fracture does not occur, and erosion occurs by plastic deformation processes. In this section, a discussion is presented of the theories that have been used to explain plastic processes in ceramic materials; these theories are applied to explain effects of particle size, impingement angle and temperature on erosion. Conditions that define the brittle to ductile transition for erosion of ceramics are also discussed.

Sheldon and Finnie (1966 a) were the first to provide a theoretical framework for understanding the transition from brittle to ductile erosion in ceramic materials. For impact that can be approximated by quasi-static loading under Hertzian loading conditions, they noted that fracture of brittle materials is described by Auerbach's law. From these relations, the condition for fracture can be expressed in terms of the maximum radius of contact and the impact load. Plastic flow

during impact is determined by the impact load and the hardness of the material. Two equations were obtained by Sheldon and Finnie (1966 a). Both related the contact load to the impact radius: one equation was for fracture ($F_m \propto a^{3/2}$); the other was for plastic deformation ($F_m \propto a^2$). At high impact loads (i.e. high particle velocities; large particle mass), the equations predict a lower load for fracture than for deformation; thus fracture dominates the impact process at high impact loads. At low impact loads the reverse is true; plastic deformation dominates the impact process. A maximum load for ductile impact was determined by setting the equations equal to one another. Following this procedure, Sheldon and Finnie (1966 a) estimated that fracture of glass occurred when the contact radius during impact was greater than ∿10μm. This estimate was about one order of magnitude greater than that observed experimentally.

A more realistic investigation of the impact problem was conducted by Evans, Gulden and Rosenblatt (1978). For sharp particle contact, Eq. (7) provides a relation between the critical load for fracture and the material parameters K_c and H. Evans et al. (1978) converted the impact load to an impact velocity using a dynamic treatment of the impact event. They showed that the critical velocity for fracture, v_c, was related to K_c and H through the following equation:

$$v_c \gtrsim (\Theta/4\pi)\ (K_c^{\,2}/r\,H^{3/2})\ (1+Z_t/Z_p)/[\rho_p(Z_t/Z_p)]^{1/2} \qquad (13)$$

where Θ is a constant (∿0.2), r is the particle radius, ρ_p is the particle density, and Z_t and Z_p are the elastic impedances of the target and particle respectively. Although Eq. (13) is only applicable to radial crack formation, the dependence of the fracture threshold on K_c, H, ρ, etc., probably also applies for lateral crack formation.

The procedure used by Evans et al. can also be applied to the elastic-plastic theory discussed by Wiederhorn and Lawn (1977) (also

see Chapter 1) to obtain the following equation for the velocity threshold:

$$v_c = (2.25\pi\tan\psi)^{-1/4} \quad (54.47/\eta^2\Theta^2)^{3/4} \quad (\alpha/m)^{1/2} \; K_c^{\,3} \; H^{-5/2} \qquad (14)$$

where η, Θ and α are constants discussed above (see eqn. 6 and 7), and 2ψ is the included angle of the contacting point of the impacting particle, (Wiederhorn and Lawn, 1979). Although these two equations are functionally different, both predict a dependence of the threshold velocity on the hardness and critical stress intensity factor of the target material, and on the size and density of the impacting particle. Both theories predict an increase in the threshold velocity for cracking as the particle size is made smaller. This prediction is in qualitative agreement with the data of Sheldon and Finnie discussed above (1966 a), which showed that a transition from brittle to ductile erosion occurs as the size of the silicon carbide particles is decreased. A closer comparison of theory and experiment is not possible, however, because Eq. (13) and (14) give threshold conditions for radial crack formation. To predict threshold conditions for erosion, a similar equation would have to be derived for lateral crack formation. Nevertheless, it is probable that the threshold velocity for lateral crack formation has a similar dependence on target and particle properties and thus also depends on stress intensity factor, hardness, and particle size and density in a way that is similar to that given in Eq. (13) and (14).

Equations (13) and (14) are useful for discussing the dependence of erosion on temperature. The critical stress intensity factor and the hardness are the only materials variables in Eq. (13) and (14) that depend on temperature; therefore, the effect of temperature on the brittle-to-ductile transition will be determined by the behavior of these variables as the temperature is increased.

Investigations of the effect of temperature on K_c suggest modest changes in K_c as the temperature is increased. Studies on sapphire (Wiederhorn,

Hockey and Roberts, 1973), for example, indicate a decrease in K_c from $\sim$2.4 MPa-$m^{1/2}$ to $\sim$1.8 MPa-$m^{1/2}$ as the temperature is increased from room temperature to 800°C. Similar results are obtained for chemical borosilicate glass (C7740) and for silica glass (C7940) (Wiederhorn, Johnson, Diness and Heuer, 1974), which showed very little change in K_c as the temperature is increased from room temperature to $\sim$600°C. On the other hand, hot pressed silicon nitride (HS-130) exhibits a substantial change in K_c as the temperature exceeds 1200°C (Evans and Wiederhorn, 1974), but this increase in K_c has been shown to be strain-rate dependent. Thus under impact loading conditions, K_c has almost the same value at 1300°C as at room temperature (Mendiratta et al., 1977, Gonazy and Johnson, 1978). A similar finding was obtained on single crystal silicon for which the ductile-to-brittle transition (determined by K_c measurements) increased from $\sim$700°C to $\sim$950°C as the loading rate increased from 5×10^{-4} cm/min to 5×10^{-2} cm/min (St. John, 1976). These results again suggest that for the dynamic loading conditions expected during impact, the critical stress intensity factor of ceramic materials is not dependent on temperature.

Measurements of the hardness of ceramic materials, however, do indicate a substantial decrease in hardness as the temperature is increased. The hardness of aluminum oxide, for example, decreases from $\sim$2000 Kg/mm^2 at room temperature to $\sim$500 Kg/mm^2 at 500°C (Westbrook, 1966). Similarly, the hardness of magnesium oxide decreases from $\sim$800 Kg/mm^2 at room temperature to $\sim$100 Kg/mm^2 at 1000°C while that of quartz decreases from $\sim$1100 Kg/mm^2 at room temperature to $\sim$200 Kg/mm^2 at 900°C (Westbrook, 1966). Similar results are obtained on other materials as the temperature is increased. Assuming that K_c remains constant as the temperature is increased, these changes

in the hardness would have significant effects on the ductile-to-brittle transition for erosion. Depending on the properties of the target material, and the theory used to predict the transition velocity, expected increases in v_c at 1000°C range from 10 to 100 times that predicted at room temperature. These increases in v_c are of the same magnitude as would be expected if the particle size were reduced by a factor of 10, as in the experiments by Sheldon and Finnie (1966 a). Studies of the erosion of ceramic materials do not support the predicted increase in v_c. For the materials investigated, temperature appears to have a small effect on the erosion rate of dense ceramic materials (Hockey, et al., 1978). Furthermore, direct examination of impact sites by transmission electron microscopy gives little indication of a significant enhancement of the plastic zone at the contact site as the temperature is increased (Hockey, et al., 1978). From this evidence we conclude that the significant parameter in Eq. (13) and (14) is not the static hardness just discussed, but the dynamic hardness (i.e., hardness measurements made using impulse load conditions).

Except for one study on soda-lime-silicate glass (Gunasekera and Hollaway, 1973), dynamic hardness measurements have not been made on ceramic materials. The study by Gunasekera and Hollaway on soda-lime-silicate glass was conducted at room temperature using load durations ranging from $\sim 10^{-3}$ to $\sim 10^{5}$ s. Over this range, the hardness of freshly cleaved glass surfaces was found to increase from ~3.5 GPa for a 10^{5} sec. load duration to ~8.5 GPa for a 10^{-3} sec. load duration. When one considers that the impulse time for small particles impacting glass surfaces is of the order of microseconds, then the importance of dynamic hardness to the erosion process becomes apparent.

Dynamic hardness measurements have been made on indium as a function of temperature (Silverio, 1963). A ballistic pendulum was used for impact times of $\sim 10^{-2}$ sec. and a falling ball for impact times of $\sim 10^{-4}$ sec. His study showed that for the temperature range -196°C to 130°C, the hardness increased as the load duration decreased. For times of $\sim 10^{-4}$ sec., a maximum value of the hardness was approached regardless of the temperature. Thus, for times less than $\sim 10^{-4}$ sec. the dynamic hardness was found to be independent of temperature. If this result could be generalized, then the ductile-to-brittle transition for the erosion of ceramics would not depend on temperature, since neither K_c, nor H in Eq. (13) and (14) would depend on temperature. Clearly, additional experimental work on dynamic K_c and H is needed to fully characterize the effect of material parameters on the erosion of ceramics.

IV. THEORIES OF EROSION

A. DUCTILE MATERIAL MODELS

The earliest consideration of ductile processes of erosion is due to Finnie (1960), who considered a micro-machining mechanism as a model. He treated the problem by assigning a plastic response character to the material through a flow stress, σ_f. The trajectory of a particle cutting and removing material was calculated, and the eroded volume, V, was determined to be given by the expression:

$$V = \frac{mv_o^2}{\sigma_f K d} g(\alpha) \qquad (15)$$

where m is the particle mass, v_o the impact velocity, K the ratio of vertical force to horizontal force on the particle, and d the depth of cut. $g(\alpha)$ is a function describing the effect of attack angle α. This approach was quite successful in explaining many features of solid particle erosion. However, quantitative discrepancies arose concerning the effect of flow stress, the velocity exponent, and the applicability of the model itself for attack angles near $\alpha = 90°$. Recent refinements of the original analysis by Finnie and McFadden (1978), in which the interaction force between the particle and the target surface is modified, have led to velocity exponents of about 2.5, which are more closely those found by experiment. Earlier, Bitter (1963) considered an indentation deformation process to occur near $\alpha = 90°$, as well as the cutting process embodied in Finnie's model. By considering the energies involved in these processes, Bitter was able to develop an expression to better account for erosion at all attack angles. This theory, as well as that

of Nielson and Gilchrist (1968) requires experimentally determined parameters for complete application. Tilly (1973) has proposed a two stage mechanism of erosion recognizing explicitly that particles impacting at near-normal incidence may fragment and the fragments may subsequently erode exposed surface features. He was able to account for a reported decrease of erosion with decreasing particle size and introduced the concept of a minimum particle size for effective erosion.

As previously described, Sheldon and Kanhere (1972) have examined the mechanism of single particle erosion of ductile materials. They then developed a method to describe the deformation and machining actions observed using indentation theory and an energy balance equation. Their results differ from previous calculations, giving the erosion volume as

$$V = K \frac{d^3 v_o^3 (\rho_p)^{3/2}}{H^{3/2}} \qquad (16)$$

where d is the (spherical) particle diameter, ρ_p the particle density, and H the Vickers hardness value of the material. This theory leads to a greater velocity dependence than expected from energy arguments (proportional to v^2).

Recent studies by Winter and Hutchings (1975) and Hutchings (1977), 1978) into the mechanisms of single particle erosion have led to suggestions of several significant impact processes and materials parameters. One important mechanism they report involves adiabatic shear (thermally localized deformation). Titanium in particular appeared sensitive to local thermal effects due to particle energy release. As a result, detachment of small metal chips took place more frequently from the ploughed metal at the impact crater in titanium than in steel specimens similarly impacted. A second consideration involves the deformation strain rate applied to a material as a result of particle impact. For small particles (<100μm) they found that high strain

rates ($\dot{\varepsilon}$) are an important consequence of impact. Calculations showed that $\dot{\varepsilon} \propto (\text{particle radius})^{-1}$, reaching values of the order of 10^7 sec^{-1} for 5μm particles and a velocity of the order of 100 m/sec. Material response at such high strain rates is not well known; such data are needed for an improved understanding. Based on single particle impact observations, Hutchings (1978) has developed a formulation of the deformation process. The two curves shown in Fig. 6 are predictions of that numerical theory using one material parameter, the indentation pressure. The original papers should be consulted for further details. It is an interesting feature of this theory that the velocity dependence of erosion varies from v_o^2 to slightly higher values depending on the detailed mechanism assumed.

Recent studies of eroded specimen structures that have been discussed in prior sections of this article show that erosive impact and wear are complex processes. It would appear that results from studies currently underway may lead to new or modified erosion models involving a more accurate understanding of the physical processes involved. An improved theoretical capability for erosion prediction should then result.

B. BRITTLE MATERIAL MODELS

Two models of erosion have been developed for brittle materials: one is based on the assumption that erosion occurs entirely by crack propagation and chipping (Sheldon and Finnie, 1966 b); the other is based on the assumption that plastic deformation contributes to the process of crack formation and surface chipping (Evans, Gulden and Rosenblatt, 1978). Erosion rates are predicted in terms of both target (fracture toughness, hardness, flaw density, etc.) and particle (velocity, density, size, etc.) properties. The models assume that particle impact is normal to the target surface, and that erosion is the result of cumulative damage of non-interacting, single particle impacts. As will be shown below, these theories predict various aspects of erosion data for ceramic materials.

The model proposed by Sheldon and Finnie (1966 b) assumes that erosion occurs as the result of Hertzian contact stresses during impact. These stresses cause cracks to grow from preexisting flaws in the target surface. The load at which crack propagation occurs is related to the distribution of surface flaws through the Weibull statistics. The approximate area, A, of cracked material is calculated for a particle penetration depth of h, and the volume removed per impact is set proportional to Ah. The final equation for the erosion rate*, W, is expressed in terms of the particle size, r, the particle velocity, v_o, and Weibull constants, m and σ_o:

$$W = k_1 r^a v^b \tag{17}$$

*Sheldon and Finnie (1966 b) expressed their results in terms of grams lost per gram of impacting particle.

where the exponents a and b are given by:

$$a = 3(m-0.67)/(m-2) \quad \text{for round particles}$$

$$a = 3.6(m-0.67)/(m-2) \quad \text{for angular particles}$$

$$b = 2.4(m-0.67)/(m-2) \quad \text{for either shape}$$

For particles much stiffer than the target, the constant, k_1, is given by:

$$k_1 = E^{0.8(m+1)/(m-2)} \rho^{1.2(m-0.67)/(m-2)} \sigma_o^{-2m/(m-2)} \tag{18}$$

where E is the modulus of elasticity of the target and ρ is the density of the particle.

Sheldon and Finnie (1966 b) compared the experimentally determined exponents, a and b, with theoretically predicted exponents and obtained satisfactory agreement for several brittle materials (glass, MgO, Al_2O_3, graphite). In a later paper, Sheldon (1970) compared experimental and theoretical value of k_1 and again found reasonable agreement between theory and experiment; however, the agreement was not as good as that for the exponents a and b. Although the theory by Sheldon and Finnie (1966 b) provides a reasonable description of erosion in brittle materials, its physical basis must be questioned because it assumes Hertzian crack formation, whereas lateral crack formation is the main cause of material removal during erosion. The recent theory by Evans et al. (1978) explains erosion in terms of experimental crack behavior during single particle impact events, and thus takes into account lateral crack formation during erosion.

The erosion model developed by Evans et al. assumes that the erosion rate is proportional to the amount of material removed by each impact event. The volume, V, lost per impact is calculated from the depth, h, of penetration and the maximum size of the lateral cracks

formed during impact. Since the lateral crack size is proportional to the radial crack size c_r, V is given by the following equation:

$$V \approx \pi c_r^2 h \tag{19}$$

Substituting semi-empirical expressions for c_r, Eq. (11), and h, Eq. (12), into Eq. (19), the following equation is obtained for the erosion rate:

$$V \propto v_o^{19/6} r^{11/3} \rho^{19/12} K_c^{-4/3} H^{-1/4} \tag{20}$$

The elastic-plastic theory used by Wiederhorn and Lawn (1979) can also be applied to the development of an erosion theory. Assuming that the lateral crack size is proportional to the radial crack size, and that the depth of the lateral cracks is proportional to the maximum particle penetration, h ($\propto m^{1/3} v_o^{2/3} H^{-1/3}$), then the following expression for the wear rate can be derived from Eq. (9) and (19):

$$V \propto v_o^{22/9} r^{11/3} \rho^{11/9} K_c^{-4/3} H^{1/9} \tag{21}$$

The velocity and particle size exponents of Eq. (17). (20) and (21)are compared with experimental data in table 1. The predicted particle size exponent is approximately the same for the three theories, the exponent for the elastic theory being slightly larger than the other two. The velocity exponents for the three theories also have similar values, the elastic theory exponent (Eq. (17)) having a value intermediate between those of the two elastic-plastic theories. The elastic-plastic theories assume the two exponents to be independent of target and particle properties, whereas the elastic contact theory predicts a dependence of the exponents on the Weibull parameter, m. The elastic-plastic theories also predict a dependence of erosion rate on target hardness and toughness, which are assumed to be the pertinent

material parameters for erosion. In contrast, the elastic theory uses the Weibull constant, σ_o, and the modulus of elasticity as the pertinent material parameters. Evans et al. (1978) have presented some experimental evidence to show that the erosion of ceramic materials depends on K_c, and H in the manner described by equation 20. Similarly, Sheldon (1970) and Sheldon and Finnie (1966b) presented evidence to support the elastic theory of erosion. Although the erosion theories discussed above are supported by erosion data, the functional dependence of these theories on material properties differ significantly, so that additional experimental testing should enable one to differentiate among the three and provide evidence as to which one more accurately describes the erosion process. Considering the complexities of the erosion process and the simplifying assumptions used to derive models of erosion, additional theoretical and experimental work will be needed to further our understanding of brittle erosion processes.

C. OTHER CONSIDERATIONS

Other processes can take place upon particle impact and should be discussed in connection with erosion mechanisms. One involves the possibility of surface melting as a result of localized energy release on impact. Smeltzer et al. (1970) studies eroded metal specimens using replica electron microscopy and reported surface structures and metal particle shapes suggesting the occurrence of local melting. Recently, Jennings et al. (1976) reported observations of surface and particle morphologies that suggested melting had occurred in erosion studies of several metals at particle velocities of 145 m/s. In addition, Christman (1977) has studies the effects of single projectile impacts on aluminum alloys. He concludes from metallographic examination that localized deformation producing intense shear bands is a characteristic feature. Studies of the surfaces of ejected metal chips revealed, in a few cases, structures suggesting that local melting (Fig. 33) was involved in the separation process for particle velocities of 185 m/s. In this example, melting was localized in the immediate area where the chip separated from the specimen surface. While high velocity particle impacts might be expected to produce such effects, this finding has not been reported by other workers in lower velocity ranges, below 100 m/s. Hutchings (1978) has estimated the expected local temperature rise based on observations of impact crater geometry. He concludes that increases of up to 500°C could occur at velocities of 100 m/s but that actual melting would appear unlikely. Such a phenomena would of course be more probable under conditions of high temperature erosion provided that surface films were penetrated.

Reports of correlations between erosion rate and other physical properties of materials have also appeared. Ascarelli (1971) introduced a quantity "thermal pressure" which is proportional to the product $\beta K \cdot \Delta T$. Here β is the linear thermal expansion coefficient, K is the bulk modulus, and ΔT the difference between the exposure temperature and the melting temperature of the material being eroded. He reported an inverse proportionality of this quality with volume erosion rates of many metals. Hutchings (1975) has noted a similar correlation for the quantity $C_p \rho \Delta T$ where C_p is the material specific heat and ρ the density. There are not sufficient data available on alloys to test either of these correlations further, and possible mechanisms involving such parameters have not been developed.

Studies of erosion at elevated temperatures have been carried out to a limited extent in recent years. However, it has not yet proven possible to develop an adequate theory giving the temperature dependence of erosion rate. In most cases environmental reactions also take place, producing surface films on the material or otherwise complicating the analysis. Further experimental work will be required in relatively simple systems in order to clarify this issue. In particular, microscopic characterization of the subsurface deformation structures should be revealing, particularly in comparison to the structures found on room temperature erosion (Ives and Ruff, 1978 a, b). It is also apparent that the erosion dependence on attack angle, particle velocity and other parameters may be significantly different at elevated temperatures than at 20°C (Finnie et al., 1978).

As indicated earlier in this review, erosion is one form of material wear and as a result there may be similar processes involved in other types of wear. In particular, two-body abrasive wear theories have previously invoked the occurrence of similar particle cutting and plowing processes (Rabinowicz, 1970) to those thought to be involved in erosion. Geometrically, however, abrasive wear involves only tangential interactions between the particles and contact surface. Comparative studies of wear debris, wear surface and subsurface structures produced by different wear modes have not been reported, although such comparisons would be of interest. A current study of erosion and abrasion in mild steel (Ruff, 1978) has indicated some potential connections. Figure 34 shows the structure of an abraded surface and the recovered wear debris resulting from dry, two-body abrasion using 50μm Al_2O_3 particles. These results can be compared with those from solid particle erosion, shown in Fig. 27 involving the same metal using the same abrasive. It appears that in both cases, much of the wear debris is produced from plastically displaced material associated with the impact craters and the abrasion grooves on the exposed surfaces. Subsurface structure comparisons are being conducted for these same exposures.

V. SIGNIFICANT PARAMETERS

The general question of material parameters, of both eroded and eroding materials, and their effect on erosion rate is of considerable interest. Indentation hardness of the eroded material is a commonly used and yet apparently insufficient parameter. Recent interest has turned to more thorough studies of all involved material characteristics, and hopefully some improved understanding will soon emerge. The additional complexities of environmental reactions and elevated temperature exposures, where surface film formation is a significant, competitive process, are presently under investigation in several laboratories.

A. ERODING PARTICLE CHARACTERISTICS

Many of the important properties of the eroding particles that determine erosion rates have been mentioned in earlier sections. However, the relative importance of various parameters are not yet agreed upon in the literature and a listing here with brief comment seems valuable. The particle characteristics that seem to be most important to the erosion process are as following (see also Finnie, 1972, Uuemois and Kleis, 1975):

1. Particle shape -- For both ductile and brittle materials, more effective erosion is generally found to be associated with angular particles (Finnie, 1960). Some basic understanding of rake angle effects is emerging for ductile materials (Hutchings, 1977a).

2. Particle size -- For ductile materials, relative erosion is essentially independent of particle size for sizes greater than a critical value. Smaller sizes are less effective and a lower threshold size ($\sim$5μm) for any erosion has been suggested.

   For brittle materials, a strong dependence of erosion rate and strength degradation on particle size is predicted and some confirmation of these predictions has been obtained. Further work is required to fully characterize the effect of particle size on the erosion of brittle materials.

3. Particle hardness -- For ductile solids, so long as the target surface hardness is much less than the particle hardness, little effect is expected except indirectly through particle fragmentation, or other changes. Theories of brittle erosion assume the particle to be harder than the target; however, for many ceramic materials, this assumption is not valid. Experimental data by Gulden (1978) suggest that particle hardness may be an important variable that

must be considered when characterizing the wear of brittle materials.

4. Particle frangibility -- For ductile materials, the effect of particle fragmentation to provide additional erosion loss has been described by Tilly (1973) and recently studied by Maji and Sheldon (1978). The increased erosion potential of abrasives due to water or impurity content may derive from an altered tendency to fragment (Uuemois and Kleis, 1975). Particle frangibility has not been considered as variable in the erosion of brittle materials, although it is known to occur in these materials (Evans and Wilshaw, 1977).

B. ERODED MATERIAL CHARACTERISTICS

Many of the material parameters considered for the erosion behavior of materials are equally involved in other modes of wear. These include:

1. Surface hardness -- the single parameter most often chosen to describe ductile material erosion rate variation (see Fig. 13). Within one alloy system, indentation hardness is frequently not a valid parameter to describe erosion differences. However, Sheldon (1977) has suggested that fully abraded surface hardness may be a more suitable quantity. As noted in this review, dynamic hardness is probably the more appropriate variable for characterizing the erosion of either ductile or brittle materials.
2. Strain-rate sensitivity -- recent single particle studies on metals (Winter and Hutchings, 1975; Hutchings, 1977) indicate that the high strain rates associated with particle erosion may lead to different deformation modes in different materials. This material characteristic has not been examined thoroughly for either ductile or brittle materials.

3. Grain orientation and grain size effects -- no systematic studies of the details of these characteristics are available for solid particle erosion processes. However, Preece et al. (1978) have recently studied such microstructural effects on cavitation erosion.

4. Surface thermal parameters -- correlations between erosion rates on the one hand, and thermal conductivities and specific heats on the other hand, have been noted, but detailed explanations are not available.

5. Toughness -- Because brittle materials erode by elastic-plastic processes, the dynamic toughness (dynamic K_{IC}) plays an important role in the wear of brittle materials. Measurements of dynamic K_{IC} are needed, both to rank brittle materials and to develop a better understanding of the process of brittle erosion.

C. ENVIRONMENTAL EFFECTS

Some remaining significant considerations are:

1. Impact energy release, surface heating and possible local melting -- temperature effects on deformation may be important in many cases. Otherwise thermal effects may only be significant for high temperature erosion.
2. Abrasive bonding to the eroded surface -- the possibility of chemical reaction and bonding to the eroded surface has been noted in the literature for high temperature erosion processes. This effect can significantly effect the erosion rate, offering protection from mechanical damage at the possible expense of chemical attack on the exposed surface.
3. Atmospheric reaction -- the formation of substantial films on exposed surfaces due to chemical reaction would be expected in actual elevated temperature exposures. It has been reported that such films can alter erosion rates, particularly for smaller particle sizes that are of the same order as the film thickness. This factor is discussed in Chapter 7.

VI. SUMMARY AND RECOMMENDATIONS

The aim of this review has been to examine briefly the current state of information on solid particle erosion phenomena. Most recently, careful studies of single particle impact processes and of the microstructure of the impacted, deformed region have produced new information that suggest basic erosion mechanisms. It is clear that except for the simplest conditions, many different processes are involved; plastic deformation over a wide range of strain rates, thermal effects, crack growth, environmental effects, and others. However, an improved understanding of the important aspects of the erosion problem seems to be emerging. That understanding should greatly aid materials designers, even though some applications problems may always require empirical and statistically based approaches. Analytical prediction capability of erosion rates under small variation of conditions may reasonably be expected in the near future.

In a rapidly developing field it is difficult to recommend detailed areas for concentrated activity. New information is accumulating too rapidly for useful recommendations at this time. However, some areas can be mentioned that either have lacked much attention or have yielded such valuable information as to be worthy of continued examination.

These would include:

-- the dynamic effects of impact on materials

-- the response of complex material microstructures to impact

-- the effects of substantial surface films on erosion

-- the role of material toughness and plastic flow properties

-- the effect of environment on erosion

Acknowledgements

Discussions with several staff members at NBS, particularly B. Hockey and L. K. Ives, on the subject of materials erosion are gratefully acknowledged. One of the authors (SMW) gratefully acknowledges support of the Office of Naval Research.

Table 1. Comparison of velocity and particle size exponents for various brittle erosion theories

$$w = k\, r^{a}\, v_{o}^{b}$$

Theory	a	b
Elastic (Eq.(17))	∿4-4.2	∿2.6 - 3
Elastic-Plastic (Eq.(20))	3.7	3.2
Elastic-Plastic (Eq.(21))	3.7	2.4
Experiment	3 - 4	2 - 4

REFERENCES

Ascarelli, P. (1971). Army Materials and Mechanics Research Center Report No. TR-71-47.

Ashford, J. P. (1968), Special Ceramics - 4, The British Ceramic Research Association (Stoke-on-Trent).

Auerbach, F., (1891), Ann. Phys. Chem., 43, 61.

Bitter, J. G. A. (1963). Wear 6, 5-21, and 6, 169-190.

Chaudhri, M. M., and Walley, S. M., (1978), Fracture Mechanics of Ceramics - 3. Flaws and Testing, Plenum Press (New York).

Christman, T. K. (1977). Thesis, Ohio State University. P. Shewmon, Advisor.

Engel, P. A. (1976). Impact Wear of Materials, Elsevier, N.Y.

Evans, A. G., (1973), J. Am. Ceram. Soc. 56, 405-9.

Evans, A. G. and Wiederhorn, S. M. (1974), J. Mat. Sci., 9, 270-278.

Evans, A. G. and Wilshaw, T. R., (1976), Acta Met. 24, 939-56.

Evans, A. G. and Wilshaw, T. R., (1977), J. Mat. Sci., 12, 97-116.

Evans, A. G., Gulden, M. E., and Rosenblatt, M. E., (1978), Proc. Roy. Soc., in press.

Finnie, I. (1960), Wear 3, 87-103.

Finnie, I., Wolak, J. and Kabil, Y. (1967). J. of Materials 2, 682-700.

Finnie, I. (1972). Wear 19, 81-90.

Finnie, I. (1978). Proceedings of the ASTM Symposium "Erosion: Prevention and Useful Applications," STP 664.

Goebel, J. A. and Pettit, F. S. (1976). Pratt and Whitney Report No. 75-200-7107-3. See also Walker, D.A., Williams, M.C., and House, R.D. (1975). Proceedings of the Minnesota Symposium on Laser Anemometry. (U. Michigan).

Goebel, J. A. Pettit, F. S. and Spriggs, D. R. (1976). Pratt and Whitney Report No. 75-200-7107-4.

Gonczy, S. T. and Johnson, D. L. (1978), Fracture Mechanics of Ceramics - 3, Flaws and Testing, Plenum Press (New York).

Goodier, J. W. (1965), Proceedings of the Seventh-Hypervelocity Impact Symposium, 3, 215.

Goodwin, J. E., Sage, W., and Tilly, G. P. (1969). Proc. Inst. Mech. Engrs. 184, 279-292.

Grant, C. and Tabakoff, W. (1975), J. Aircraft 12, 471-478.

Gunasekera, S. P. and Holloway, D. G. (1973) Phys. Chem. Glasses, 14, 45-52.

Gulden, M. E., (1978), Proccedings of the ASTM Symposium, "Erosion: Prevention and Useful Applications," STP 664.

Hockey, B. J., (1971), J. Amer. Ceram. Soc 54, 223.

Hockey, B. J., and Lawn, B. R., (1975), J. Matls. Sci. 10, 1275.

Hockey, B. J., Wiederhorn, S. M. and Johnson, H., (1978), Fracture Mechanics of Ceramics - 3, Flaws and Testing, Plenum Press (New York).

Hutchings, I. M. and Winter, R. E. (1974). Wear 27, 121-128.

Hutchings, I. M. and Winter, R. E. (1975). J. Phys. D: Appl. Phys., 8, 8-14.

Hutchings, I. M. (1977a). Int. J. Mech. Sci. 19, 45-52.

Hutchings, I. M. (1977b). J. Phys. D: Appl. Phys. 10, 179-183.

Hutchings, I. M. (1978). Proceedings of the ASTM Symposium "Erosion: Prevention and Useful Application," STP 664.

Ives, L. K. (1977). J. Engrg. Matls. and Tech., Trans ASME 99, 126-132.

Ives, L. K. and Ruff, A. W. (1978a). Wear 46, 149-162.

Ives, L. K. and Ruff, A. W. (1978b). Proceedings of the ASTM Symposium "Erosion: Prevention and Useful Applications", STP 664.

Kirchner, H. P. and Gruver, R. M., (1977), Mat. Sci. and Engr., 28, 153-60.

Langitan, F. B., and Lawn, B. R., (1970), J. Appl. Phys. 41, 3357.

Lawn, B. R. and Swain, M. V., (1975), J. Mater. Sci., 10, 113.

Lawn, B. R. and Wilshaw, T. R. (1975), J. Mater. Sci., 10, 1049-81.

Lawn, B.R., and Fuller, E.R., (1975), J. Mater. Sci., 10, 2016-24.

Lawn, B. R., and Evans, A. G., (1977), J. Mater. Sci., 12, 2195-99.

Lawn, B. R. and Marshall, D. B., (1978), Fracture Mechanics of Ceramics - 3, Flaws and Testing, Plenum Press (New York).

Levy, A. V. (1978), Private Communication.

Maji, J. and Sheldon, G. L. (1978). Proceedings of ASTM Symposium "Erosion: Prevention and Useful Applications", STP 664.

Mendiratta, M. G., Wimmer, J., Bransky, J. (1977), J. Mat. Sci., 12, 212-214.

Mills, D. and Mason, J. S. (1977). Wear 44, 311-328.

National Research Council (1977). Erosion Control in Energy Systems, pp.228.

Neilson, J. H. and Gilchrist, A. (1968). Wear 11, 111-122.

Preece, C. M. and Macmillan, N. H. (1977). Ann. Review of Materials Science

Preece, C.M., Vaidya, S., and Dakshiramoorthy, S. (1978), Proceedings of ASTM Symposium "Erosion: Prevention and Useful Applications", STP 664.

Rabinowicz, E. (1965). Friction and Wear of Materials, J. Wiley and Sons, N.Y.

Roesler, F. C. (1956) Proc. Phys. Soc., London, Sect. B, 69, 981-92.

Ruff, A. W. and Ives, L. K. (1975). Wear 35, 195-199.

Ruff, A. W. (1976). Wear 40, 59-74.

Ruff, A.W. (1978). International Conference on Fundamentals of Tribology, MIT, Cambridge, Mass. Also unpublished work.

Sheldon, G. L. (1970). Trans. ASME: J. Basic Engr., 92, 619-26.

Sheldon, G. L. (1977). J. Engrg. Matls. and Tech., Trans ASME 99, 133-137.

Sheldon, G. L., and Finnie, I. (1966a) Trans ASME: Journal of Engineering for Industry, 88, 387-92.

Sheldon, G. L. and Finnie, I., (1966b) Trans. ASME: Journal of Engineering for Industry, 88, 393-400.

Sheldon, G. L., and Kanhere, A. (1972). Wear 21, 195-208.

Shelton, H., Hendricks, C. D. and Weuker, R. F. (1960). J. Appl. Phys., 31, 1243.

Silverio, A. (1963) Ph.D. Dissertation, Cambridge, reported in The Friction and Lubrication of Solids - II, by F. E. Bowden and D. Tabor, Oxford University Press, 1964.

St. John, C. (1975) Phil. Mag., 32, 1193-1212.

Smeltzer, C. E., Gulden, M. E., and Compton, W. A. (1970). J. Basic Engrg., Trans ASME 92, 639-654.

Tilly, G. P. (1969). Wear 14, 63-79.

Tilly, G. P. (1973). Wear 23, 87-96.

Uuemois, H. and Kleis, I. (1975). Wear 31, 359-371.

Westbrook, J. H. (1966), Rev. Hautes Temper. et Refract., 3, 47-57.

Westbrook, J. H. and Conrad, H., editors, (1973), The Science of Hardness Testing and Its Research Applications, American Society of Metals, Metals Park, Ohio.

Wiederhorn, S. M., Hockey, B. J., and Roberts, D. E. (1973), Phil. Mag., 28, 783-96.

Wiederhorn, S. M., Johnson, H., Diness, A. M., and Heuer, A. H. (1974), J. Am. Ceram. Soc. 57, 336-41.

Wiederhorn, S. M., and Lawn, B. R. (1977), J. Am. Ceram. Soc., 60, 451-8.

Wiederhorn, S. M., Fuller, E. R., Jr., Bukowski, J. M., and Robbins, C. R. (1977), Trans ASME Journal of Engineering Materials and Technology, 99, 143-46.

Wiederhorn, S. M., and Lawn, B. R. (1979), J. Amer. Ceram. Soc., January/February issue.

Winter, R. E. and Hutchings, I. M. (1974). Wear 29, 181-194.

Young, J. P. and Ruff, A. W. (1977). J. Engrg. Matls. and Tech, Trans ASME, 99, 121-125.

Zahavi, J., Wagner, H. J., and Posnansky, A. (1978). Proceedings of ASTM Symposium "Erosion: Prevention and Useful Applications," STP 664.

FIGURE CAPTIONS

Fig. 1. (a) Erosion impact craters on steel surface. (Ives et al., 1975).

(b) AISI 310 steel surface after erosion at 25°C at 40 m/s. (Ives, 1976).

Fig. 2. Schematic diagram of particle accelerator device. (Ives and Ruff, 1978a).

Fig. 3. (a) Damage in aluminum caused by 3 min. steel sphere impacting at 18.5°, 220 m/s. (Hutchings and Winter, 1974).

(b) Section through crater formed at 40°, 270 m/s. (Hutchings and Winter, 1975).

Fig. 4. Impact craters in 310 stainless steel produced by 50μm Al_2O_3 particles at 59 m/s. (a) SEM and (b) TEM micrographs of crater produced at 90° attack angle. (Ives and Ruff, 1978a).

Fig. 5. (a) Impact crater in 310 stainless steel produced by 50μm glass sphere at 20° attack angle at 59 m/s.

(b) Dislocation arrangement at rim of impact crater above. (Ives and Ruff, 1978a).

Fig. 6. Indentation volume for 30° impact on steel. Lines are theoretical (see text). (Hutchings, 1978).

Fig. 7. (a) Impact geometry and crater produced in steel. Velocity and rake angle are shown.

(b) Etched section of the crater above. Note the clear boundary between the deformed and undeformed material. (Winter and Hutchings, 1974).

Fig. 8. Schematic diagram of the type of damage that occurs when a sphere is pressed against the surface of a brittle material (Lawn and Wilshaw, 1975).

Fig. 9. Fracture damage resulting when a sphere is pressed against a glass surface (Courtesy of K. Phillips, Reported by Lawn and Wilshaw, 1975).

Fig. 10. Schematic diagram of crack growth during sharp particle impact. + sign indicates loading; - sign indicates unloading. (Lawn and Swain, 1975).

Fig. 11. Impact site in MgO produced by 65 μm Al_2O_3 particles at a velocity of 90 m/s and 90° impact angle TEM micrograph demonstrating dense tangles of dislocations at the impact site (Hockey et al., 1978).

Fig. 12. Impact site in Si produced by 65 μm Al_2O_3 particles at a velocity of 90 m/s and 90° impact angles. Although most of the deformed region has chipped out of the specimen surface, the TEM micrograph reveals residual dislocations and cracks associated with the impact site (Hockey et al., 1978).

Fig. 13. Impact site in SiC produced by 150 μm SiC particles at a velocity of 94 m/s and a 90° impact angle. (Courtesy of Hockey).

Fig. 14. Optical micrograph showing normal impact damage in Al_2O_3 produced at (2) 25°C and (b) 1000°C. (Hockey et al., 1978).

Fig. 15. Optical micrograph showing a series of shallow surface impressions produced in Al_2O_3 by 15° impingement. (Hockey et al., 1978).

Fig. 16. Transmission electron micrograph in SiC by 15° impingement. Absence of cracks and presence of dislocations confirm fully plastic nature of impact event (Hockey et al., 1978).

Fig. 17. Schematic representation of erosion rate on attack angle, (Ives and Ruff, 1978a).

Fig. 18. Influence of velocity on erosion for different materials (Goodwin et. al., 1969).

Fig. 19. Collected erosion measurements on copper. (Ives and Ruff, 1978b).

Fig. 20. Velocity dependence of erosion at 975°C and 25°C. (Ives, 1977).

Fig. 21. Influence of particle size on erosion of an 11 percent chromium steel (Goodwin et. al., 1969).

Fig. 22. Erosion of 1100-0 Aluminum at a velocity of 30.5 m/s as a function of impingement angle and temperature. Homologous temperature = T/T(melting). (Finnie et. al., 1978).

Fig. 23. Volume removal as a function of VHN for metals eroded at α=20 deg and velocities of 250 and 450 ft/sec. (No data were taken for nickel at 450 ft/sec.) All metals except cadmium were in annealed condition. (Finnie et. al., 1967).

Fig. 24. Copper specimen mass change for accumulated exposures. (Ives and Ruff, 1978b).

Fig. 25. Cross section of copper surfaces eroded at 90° and 20 m/s (a) induction period (b) steady state. (Ives and Ruff, 1978b).

Fig. 26. Al_2O_3 particle embedded in copper surface eroded at 90° and 60 m/s. (Ives and Ruff, 1978a).

Fig. 27. Scanning electron micrographs of (a) the surface of eroded 1015 steel and (b) steel debris particles recovered after erosion at 40 m/s and 30° attack angle using 50μm Al_2O_3. (Ruff, 1978).

Fig. 28. Weight loss from plate glass as a function of impingement angle, α, and particle size (Sheldon and Finnie, 1968a).

Fig. 29. Surface of plate glass after erosion by silicon carbide particles at an angle of 30° and a velocity of ∿150 m/s (Sheldon and Finnie, 1968a).

Fig. 30. Erosive wear of hot-pressed silicon nitride as a function of impingement angle. Curves represent erosion dependence for purely brittle behavior (Hockey et al., 1978).

Fig. 31. Scanning electron micrograph of surface morphology of sintered aluminum oxide after erosion at 1000°C, 90° impingement (Hockey et al., 1978).

Fig. 32. Furrow formation in sintered aluminum oxide eroded at 1000°C, 15° impingement (Hockey et al., 1978).

Fig. 33. Surface morphology on eroded aluminum alloy chips. (Christman, 1977).

Fig. 34. Scanning electron micrographs of (a) the surface of abraded 1015 steel and (b) steel debris particles recovered after wear under dry conditions at 2.2 N load. (Ruff, 1978).

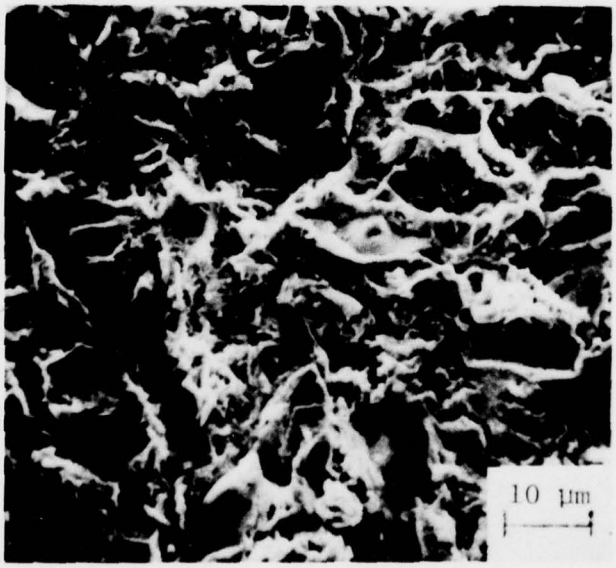

Fig. 1. (a) Erosion impact craters on steel surface. (Ives et al., 1975).

(b) AISI 310 steel surface after erosion at 25°C at 40 m/s. (Ives, 1976).

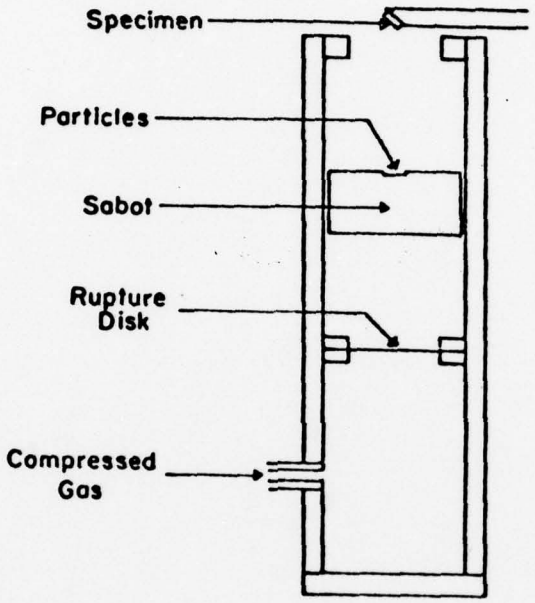

Fig. 2. Schematic diagram of particle accelerator device. (Ives and Ruff, 1978a).

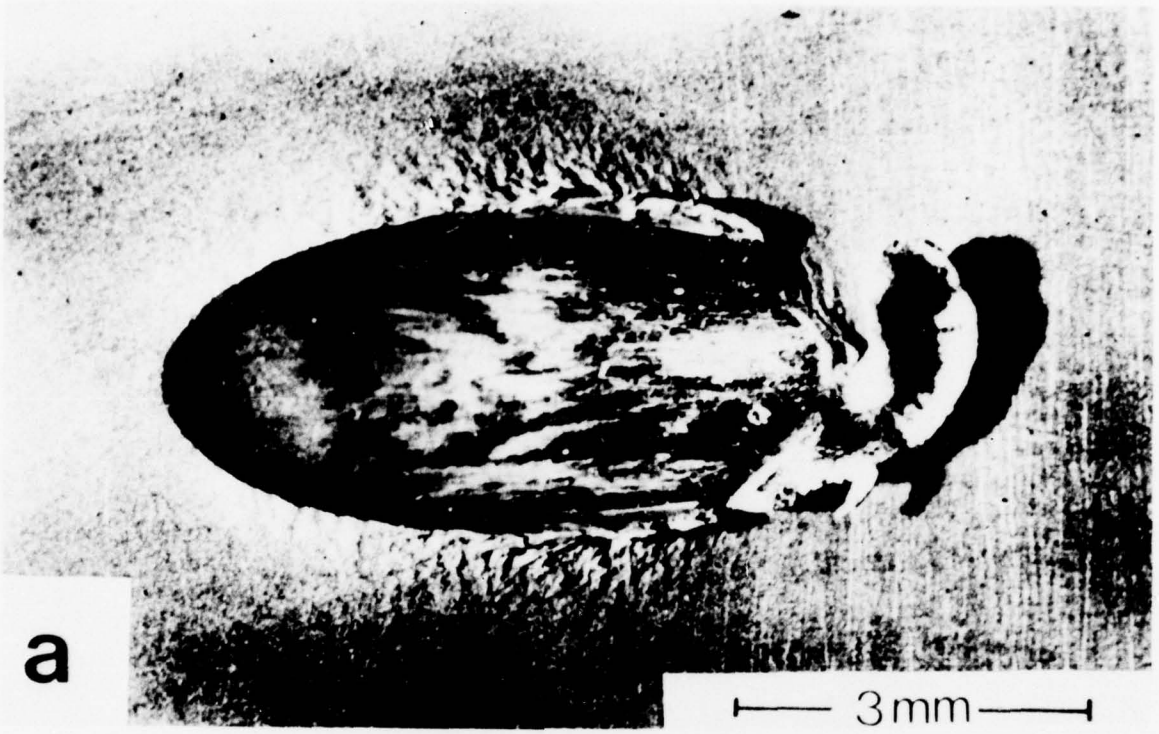

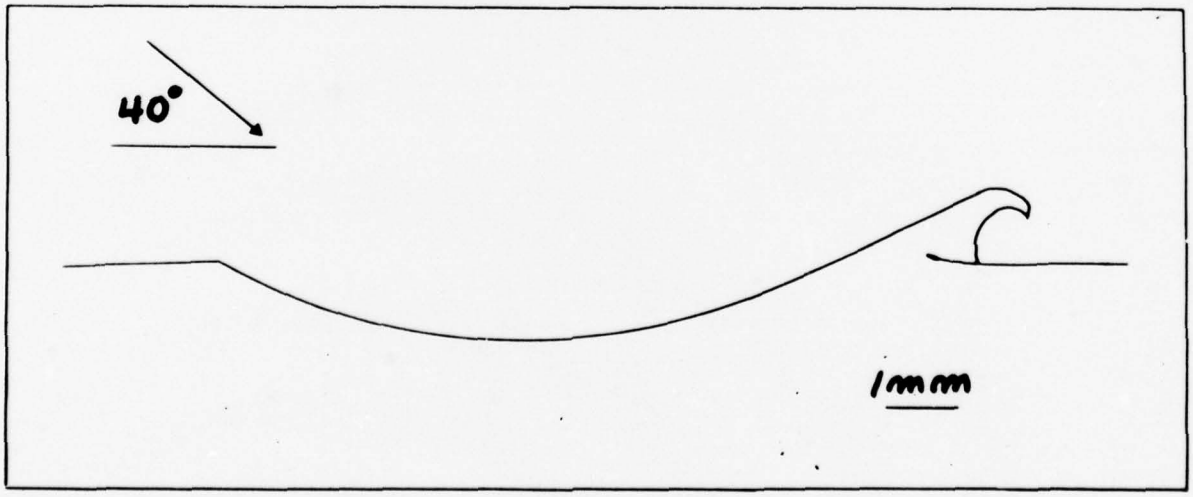

Fig. 3. (a) Damage in aluminum caused by 3 min. steel sphere impacting at 18.5°, 220 m/s. (Hutchings and Winter, 1974).

(b) Section through crater formed at 40°, 270 m/s. (Hutchings and Winter, 1975).

Fig. 4. Impact craters in 310 stainless steel produced by 50μm Al_2O_3 particles at 59 m/s. (a) SEM and (b) TEM micrographs of crater produced at 90° attack angle. (Ives and Ruff, 1978a).

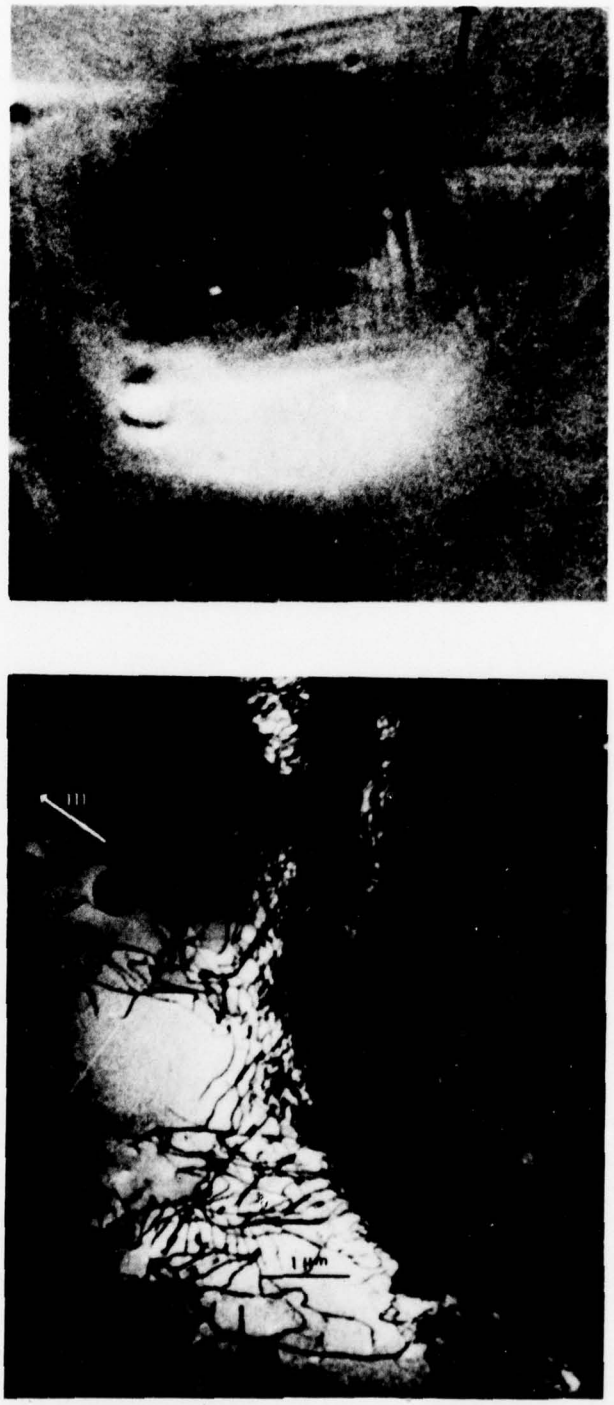

Fig. 5. (a) Impact crater in 310 stainless steel produced by 50μm glass sphere at 20° attack angle at 59 m/s.

(b) Dislocation arrangement at rim of impact crater above. (Ives and Ruff, 1978a).

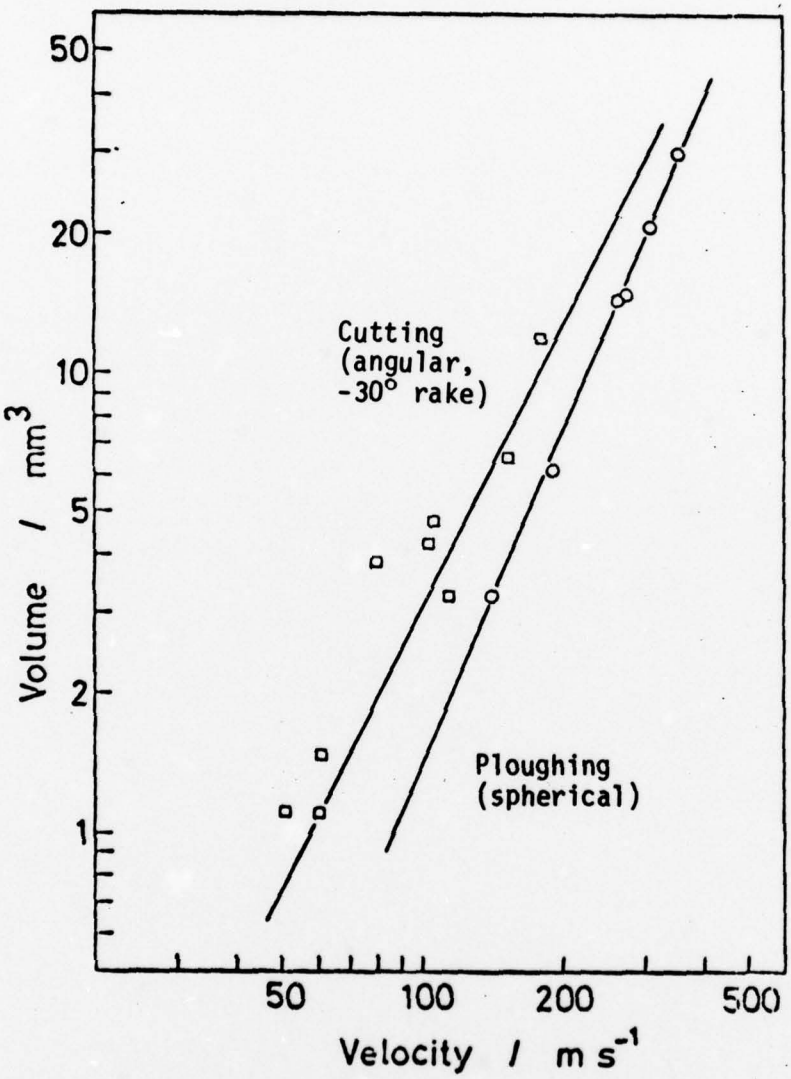

Fig. 6. Indentation volume for 30° impact on steel. Lines are theoretical (see text). (Hutchings, 1978).

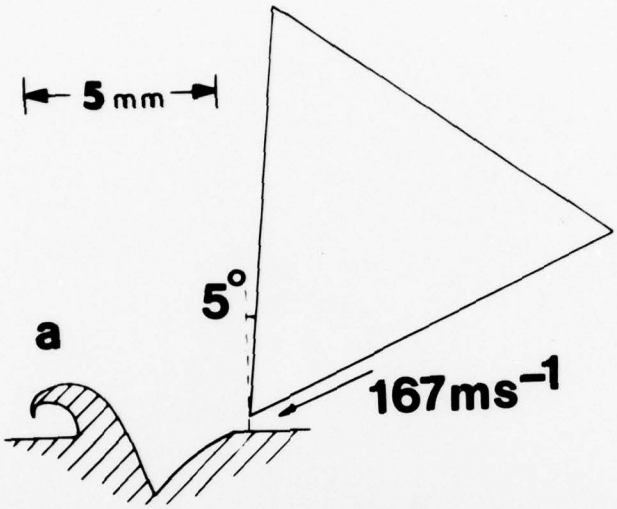

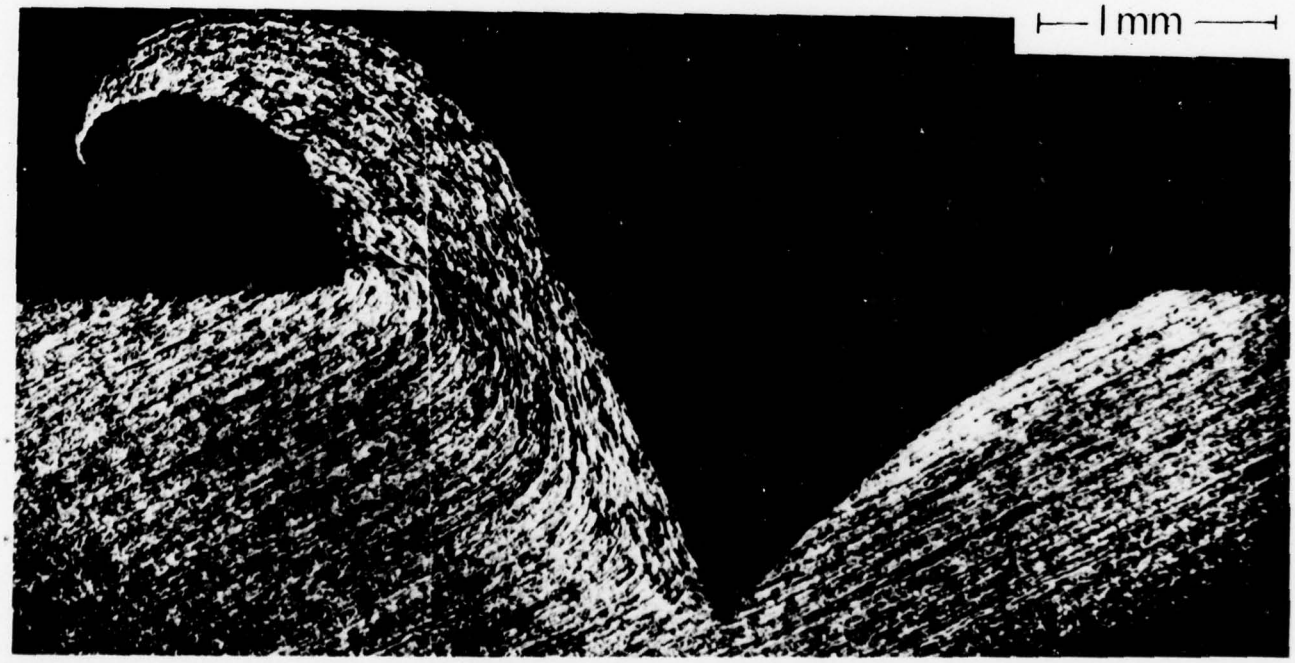

Fig. 7. (a) Impact geometry and crater produced in steel. Velocity and rake angle are shown.

(b) Etched section of the crater above. Observe the clear boundary between the deformed and undeformed material. (Winter and Hutchings, 1974).

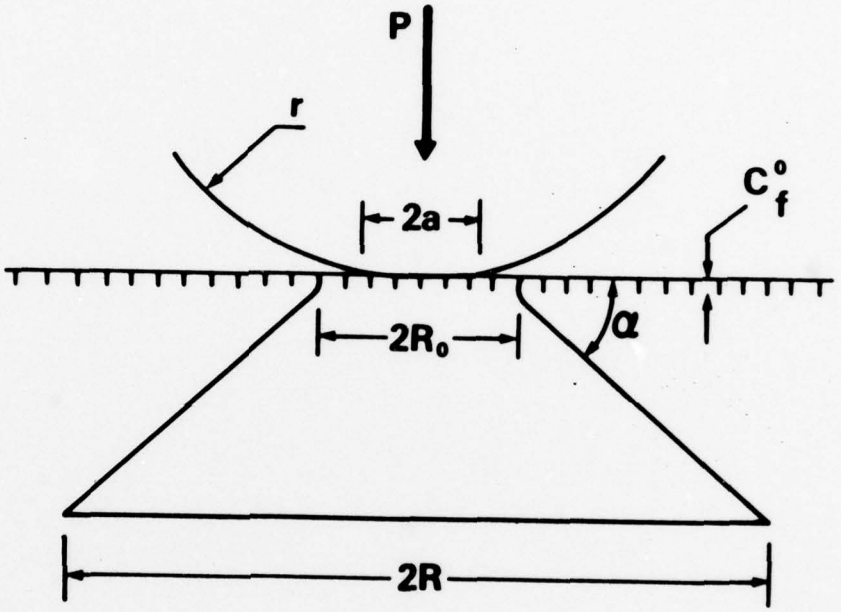

Fig. 8. Schematic diagram of the type of damage that occurs when a sphere is pressed against the surface of a brittle material (Lawn and Wilshaw, 1975).

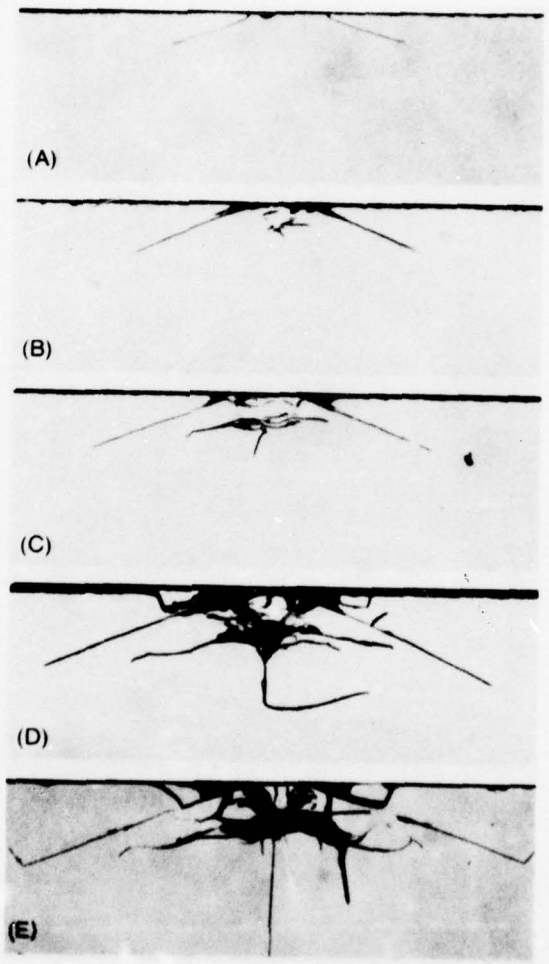

Fig. 9. Fracture damage resulting when a sphere is pressed against a glass surface (Courtesy of K. Phillips, Reported by Lawn and Wilshaw, 1975).

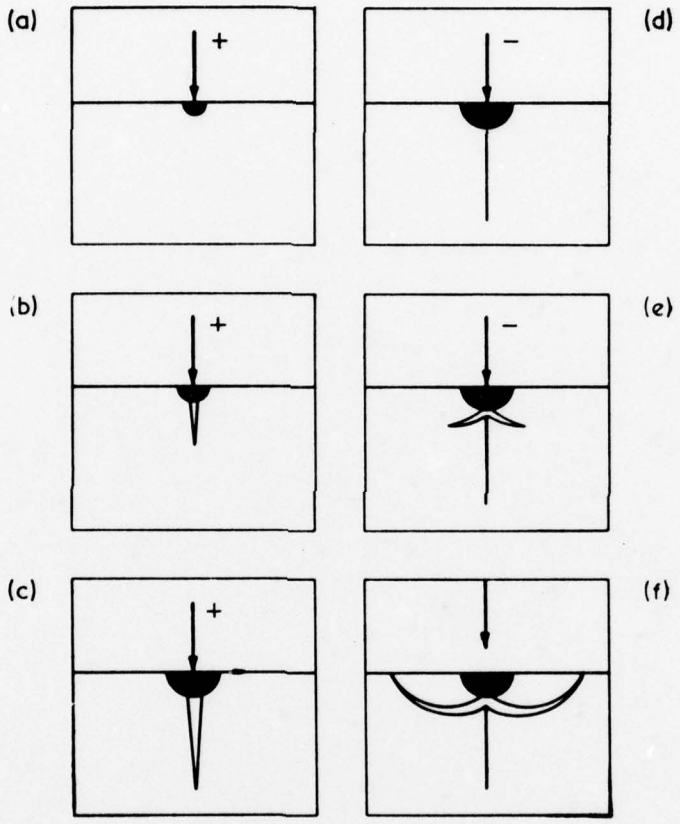

Fig. 10. Schematic diagram of crack growth during sharp particle impact. + sign indicates loading; - sign indicates unloading. (Lawn and Swain, 1975).

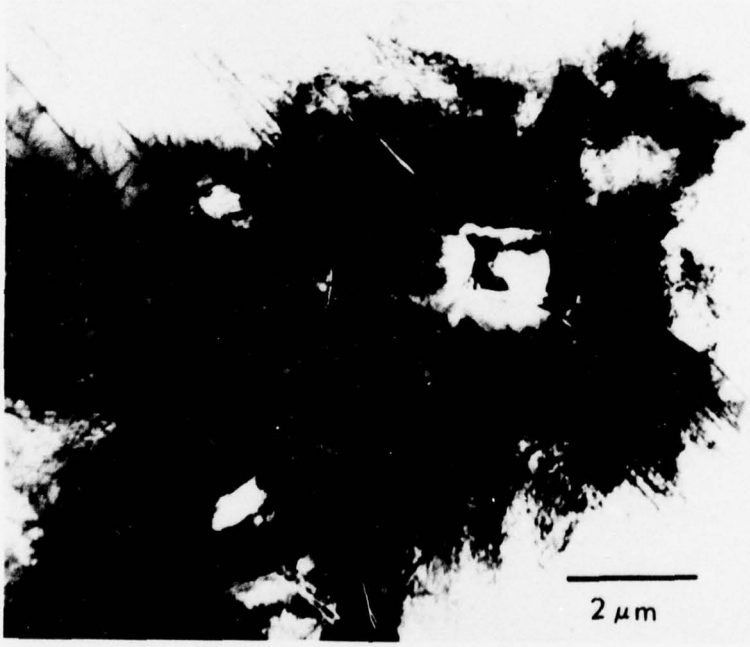

Fig. 11. Impact site in MgO produced by 150 μm SiC particles at a velocity of 90 m/s and 90° impact angle TEM micrograph demonstrating dense tangles of dislocations at the impact site (Hockey et al. 1978)

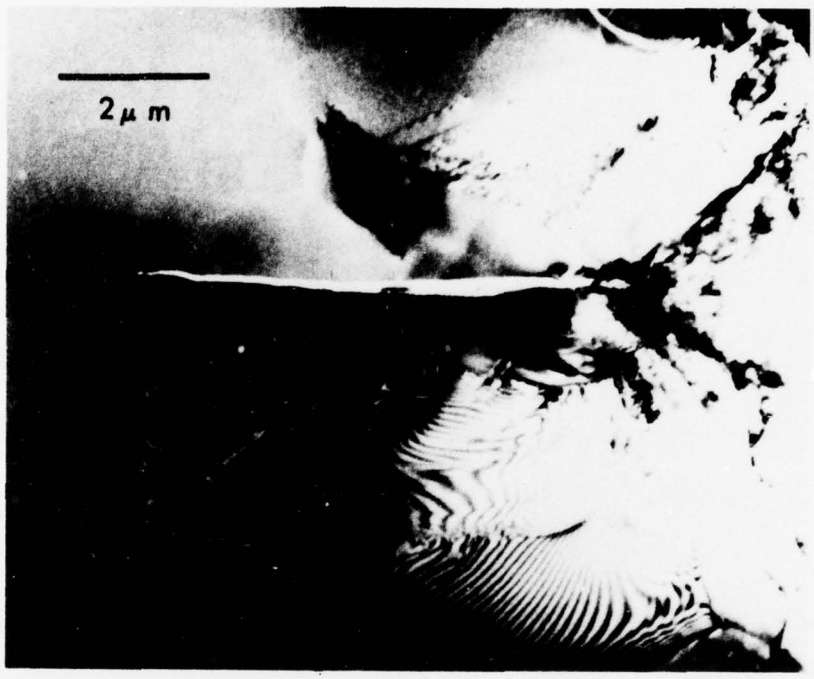

Fig. 12. Impact site in Si produced by 90 μm Al_2O_3 particles at a velocity of 90 m/s and 90° impact angles. Although most of the deformed region has chipped out of the specimen surface, the TEM micrograph reveals residual dislocations associated with the impact site (Hockey et al., 1978)

Fig. 13. Impact site in SiC produced by 150 μm SiC particles at a velocity of 94 m/s and a 90° impact angle. (Courtesy of Hockey).

Fig. 14. Normal impact damage in Al_2O_3 produced at (a) 25°C and (b) 1000°C. (Hockey et al., 1978)

Fig. 15. Optical micrograph showing a series of shallow surface impressions produced in Al_2O_3 by 15° impingement. (Hockey et al., 1978).

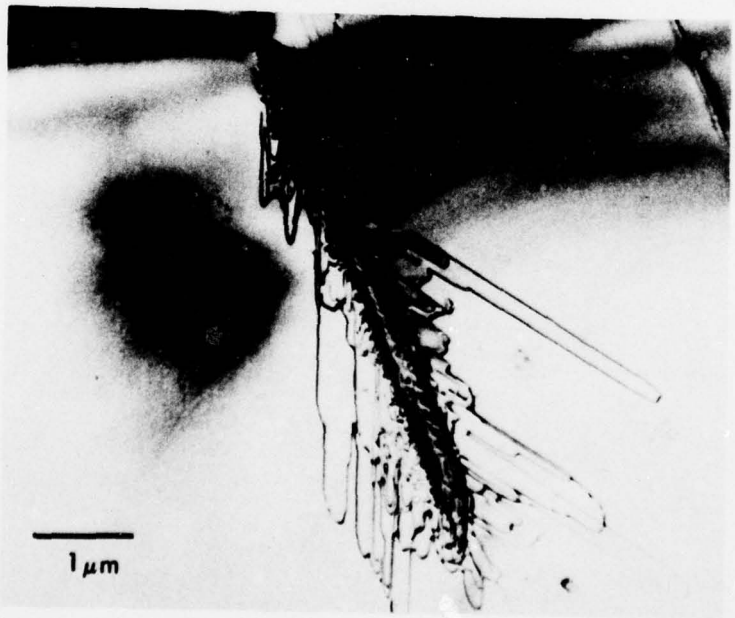

Fig. 16. Transmission electron micrograph showing region beneath shallow surface impressions produced in SiC by 15° impingement. Absence of cracks and presence of dislocations confirm fully plastic nature of impact event (Hockey et al., 1978).

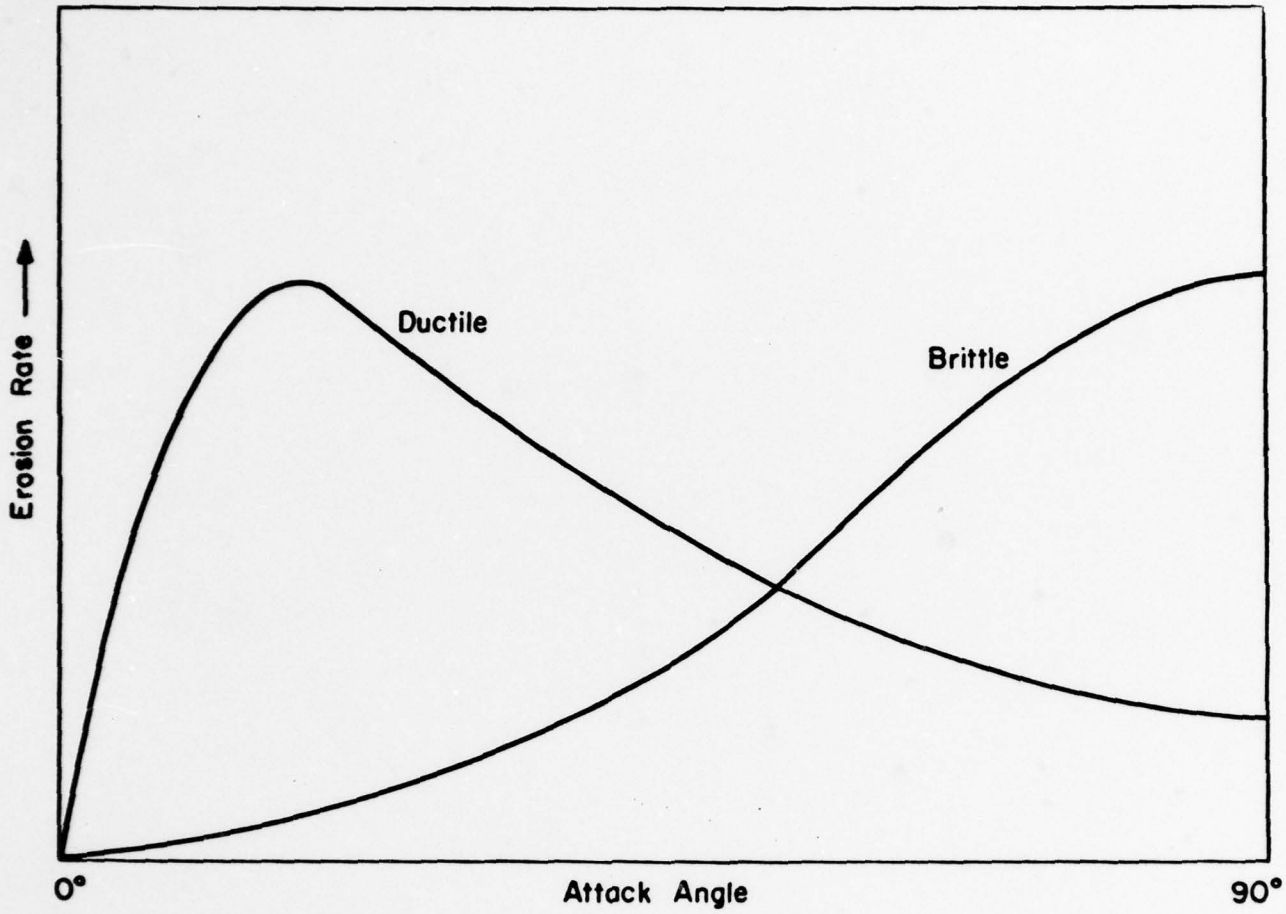

Fig. 17. Schematic representation of erosion rate on attack angle, (Ives and Ruff, 1978a).

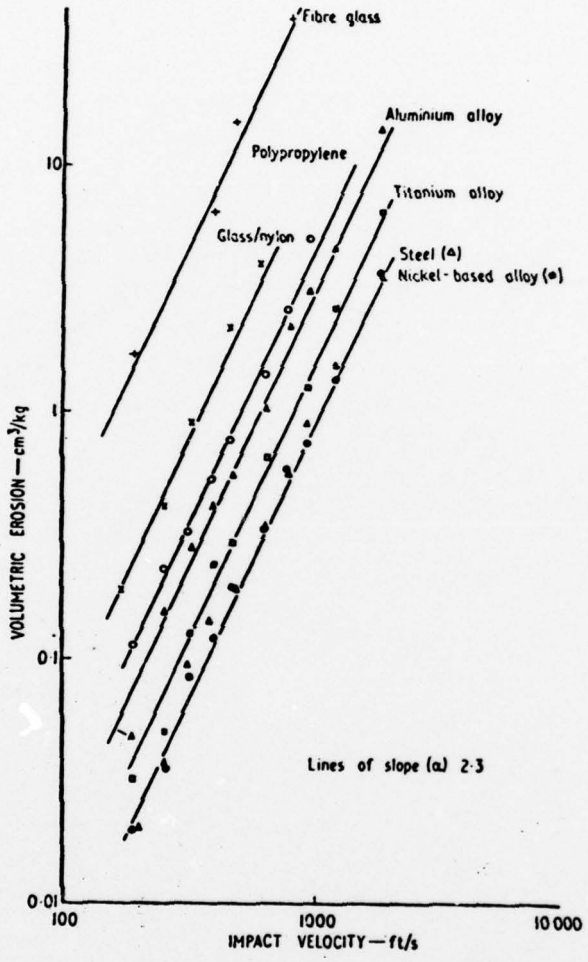

Fig. 18. Influence of velocity on erosion for different materials (Goodwin et. al., 1969).

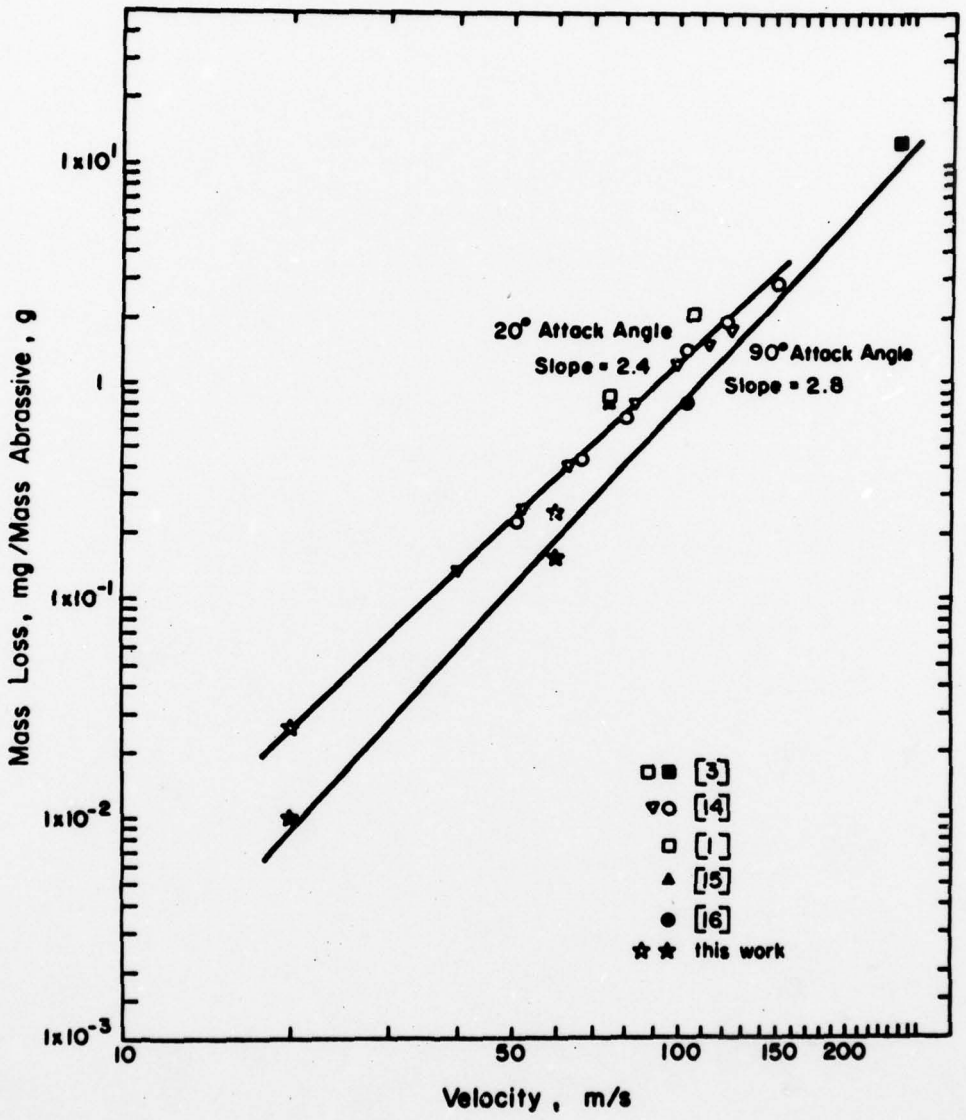

Fig. 19. Collected erosion measurements on copper. (Ives and Ruff, 1978b).

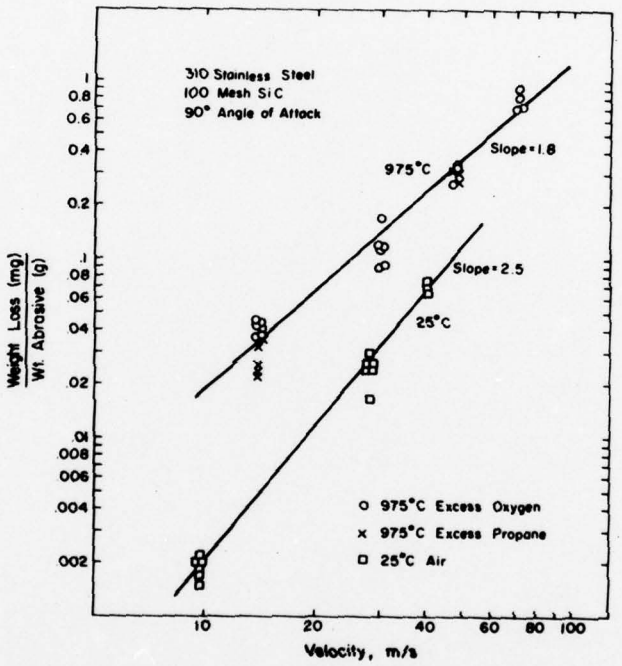

Fig. 20. Velocity dependence of erosion at 975°C and 25°C. (Ives, 1977).

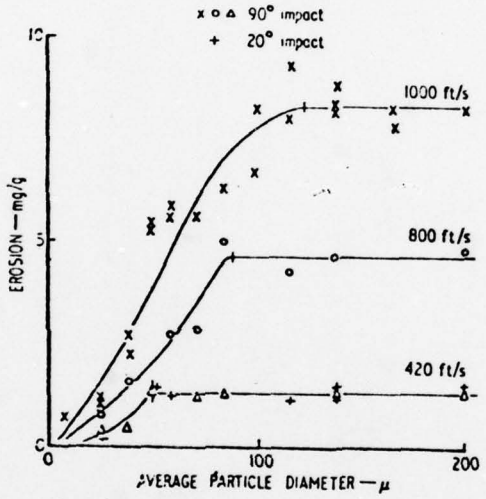

Fig. 21. Influence of particle size on erosion of an 11 percent chromium steel (Goodwin et. al., 1969).

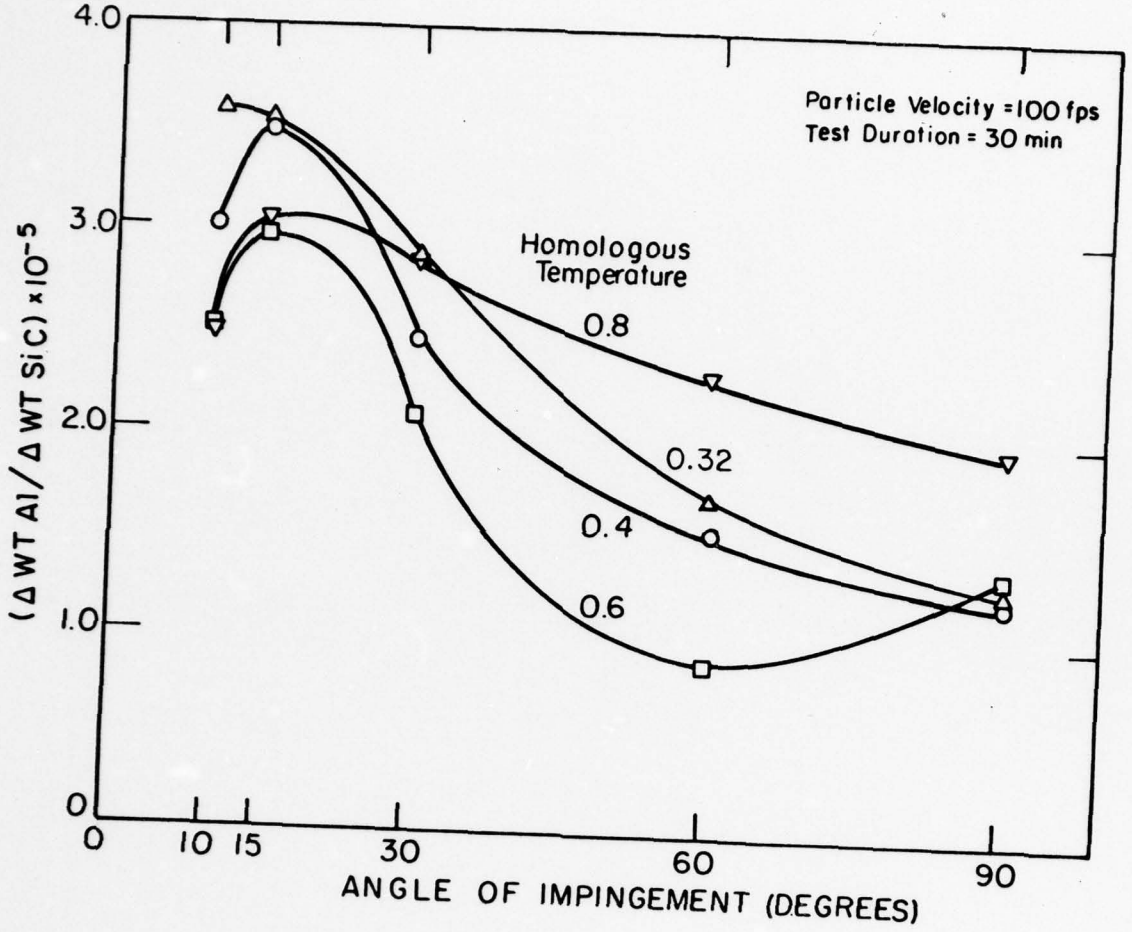

Fig. 22. *Erosion of 1100-0* Aluminum at a velocity of 30.5 m/s as a function of impingement angle and temperature. Homologous temperature = T/T(melting). (Finnie et. al., 1978).

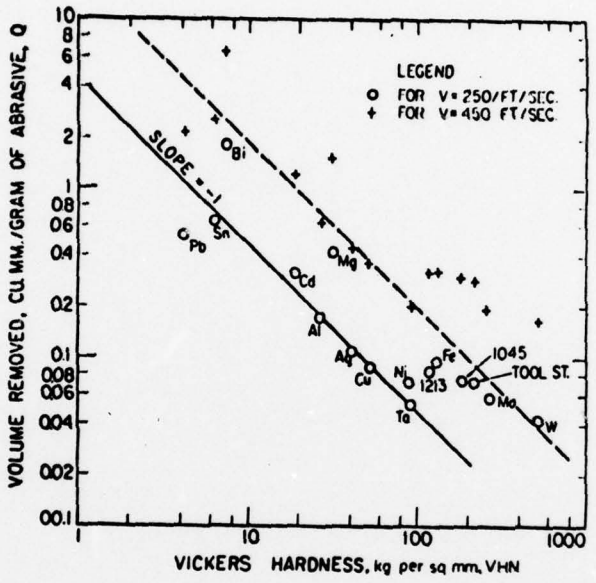

Fig. 23. Volume removal as a function of VHN for metals eroded at α=20 deg and velocities of 250 and 450 ft/sec. (No data were taken for nickel at 450 ft/sec.) All metals except cadmium were in annealed condition. (Finnie et. al., 1967).

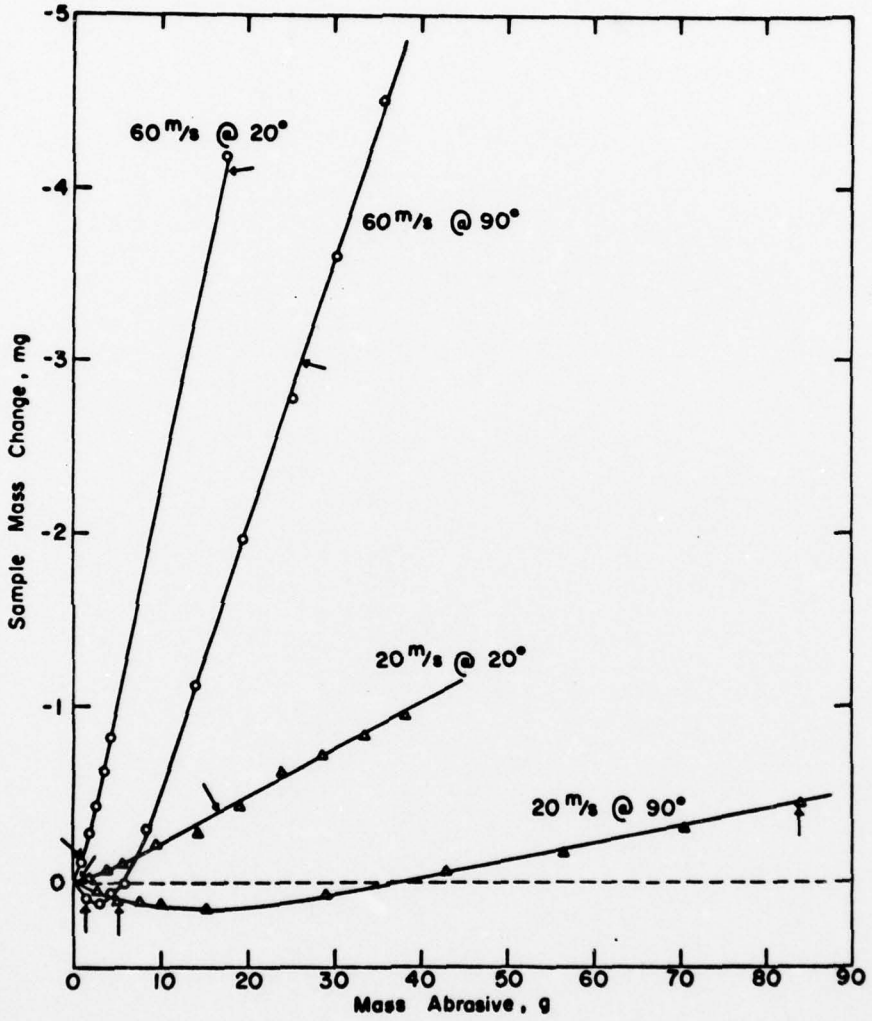

Fig. 24. Copper specimen mass change for accumulated exposures. (Ives and Ruff, 1978b).

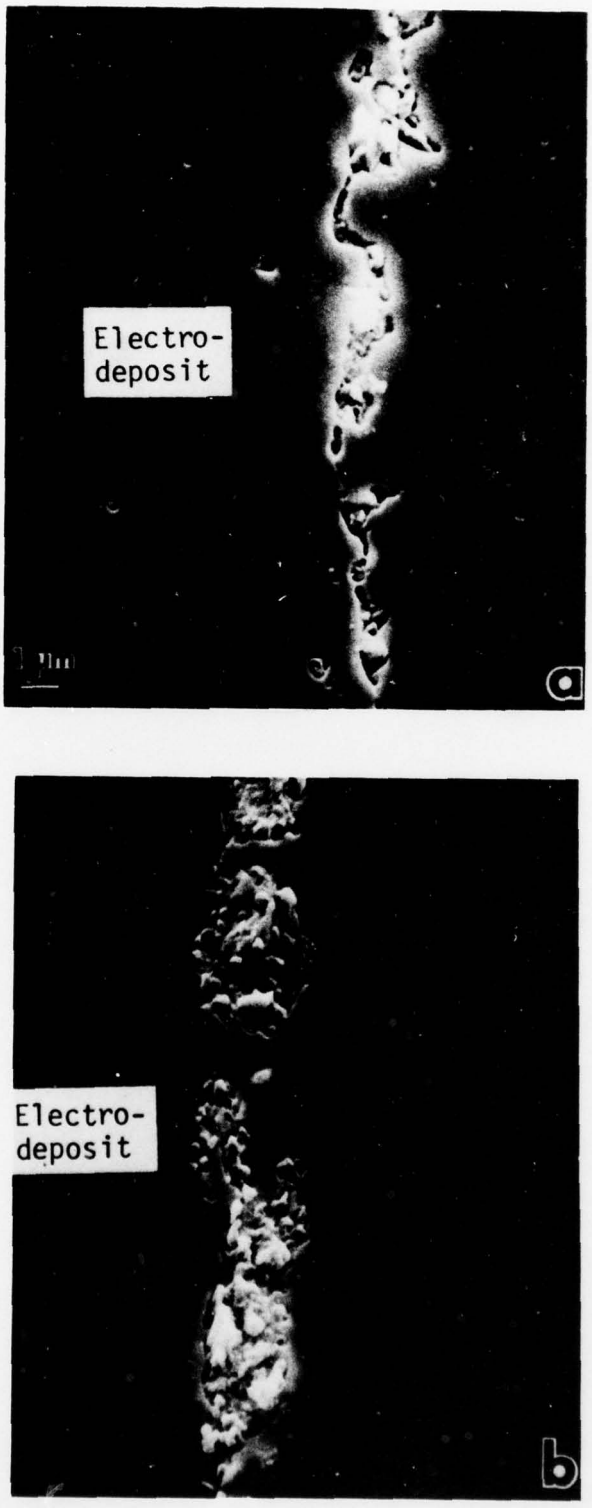

Fig. 25. Cross section of copper surfaces eroded at 90° and 20 m/s (a) induction period (b) steady state. (Ives and Ruff, 1978b).

Fig. 26. Al_2O_3 particle embedded in copper surface eroded at 90° and 60 m/s. (Ives and Ruff, 1978a).

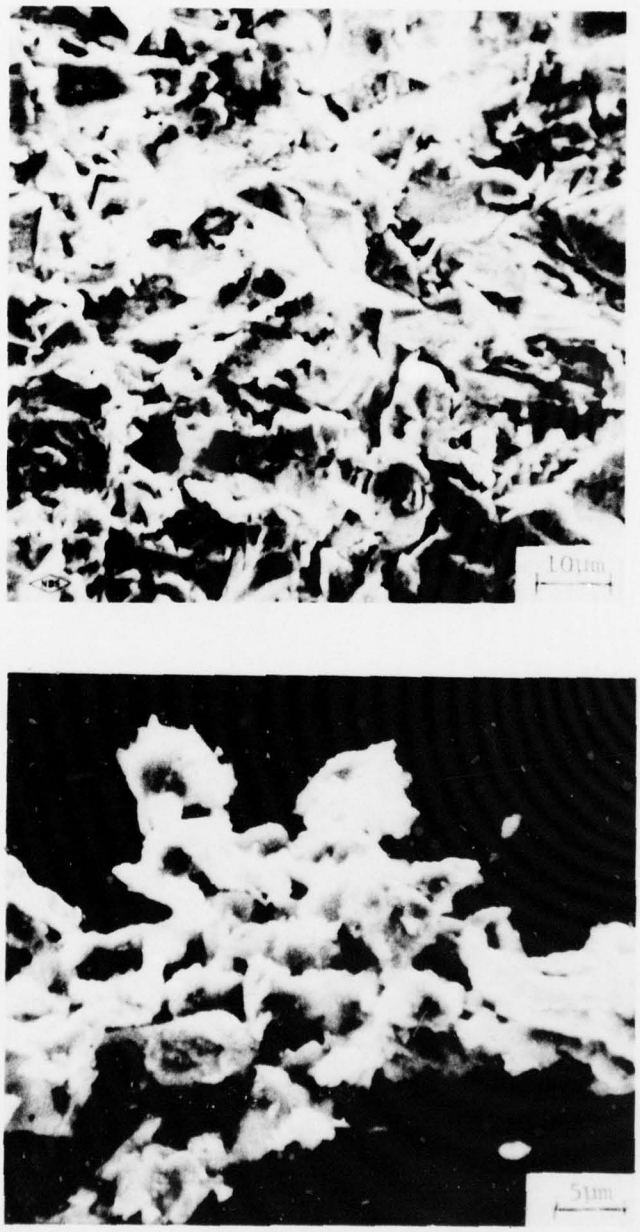

Fig. 27. Scanning electron micrographs of (a) the surface of eroded 1015 steel and (b) steel debris particles recovered after erosion at 40 m/s and 30° attack angle using 50μm Al_2O_3. (Ruff, 1978).

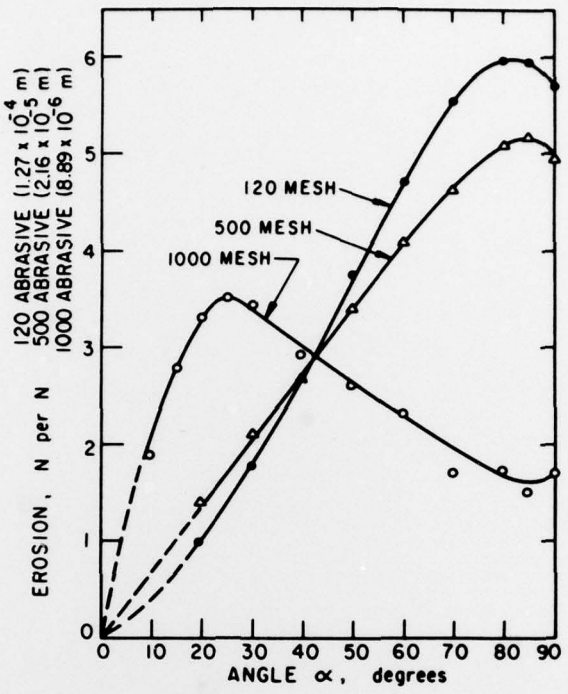

Fig. 28. Weight loss from plate glass as a function of impingement angle, α, and particle size (Sheldon and Finnie, 1968a).

Fig. 29. Surface of plate glass after erosion by 1000 mesh grit silicon carbide particles at an angle of 30° and a velocity of ∿150 m/s width of field ∿1.7 mm (Sheldon and Finnie, 1968a).

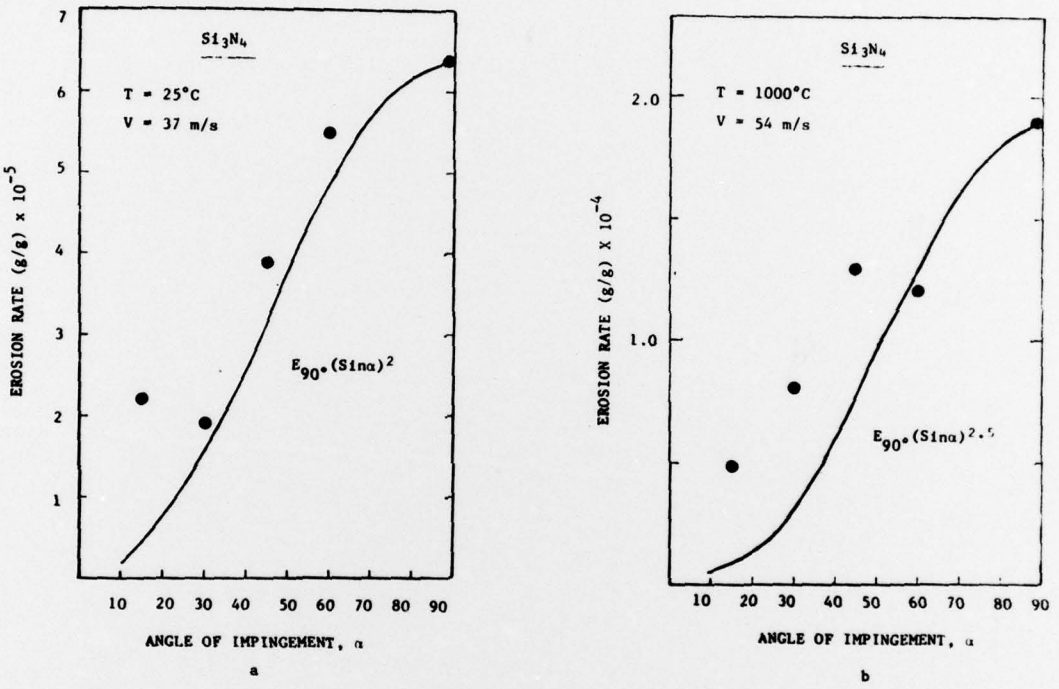

Fig. 30. Erosive wear of hot-pressed silicon nitride as a function of impingement angle. Curves represent erosion dependence for purely brittle behavior (Hockey et al., 1978).

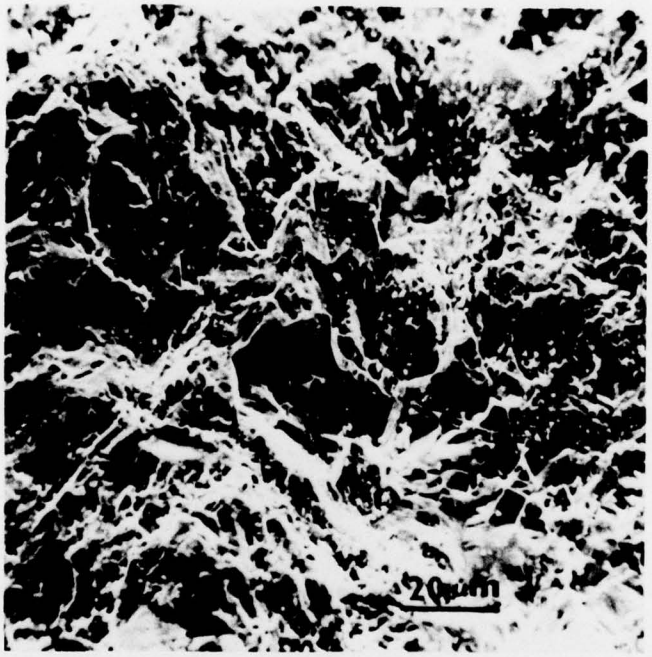

Fig. 31. Scanning electron micrograph of surface morphology of sintered aluminum oxide after erosion at 1000°C, 90° impingement (Hockey et al., 1978).

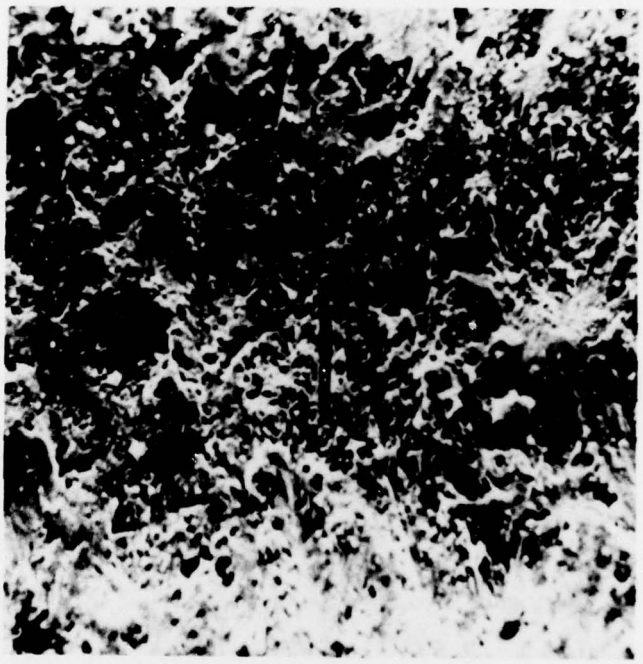

Fig. 32. Furrow formation in sintered aluminum oxide, eroded at 1000°C, 15° impingement (Hockey et al., 1978).

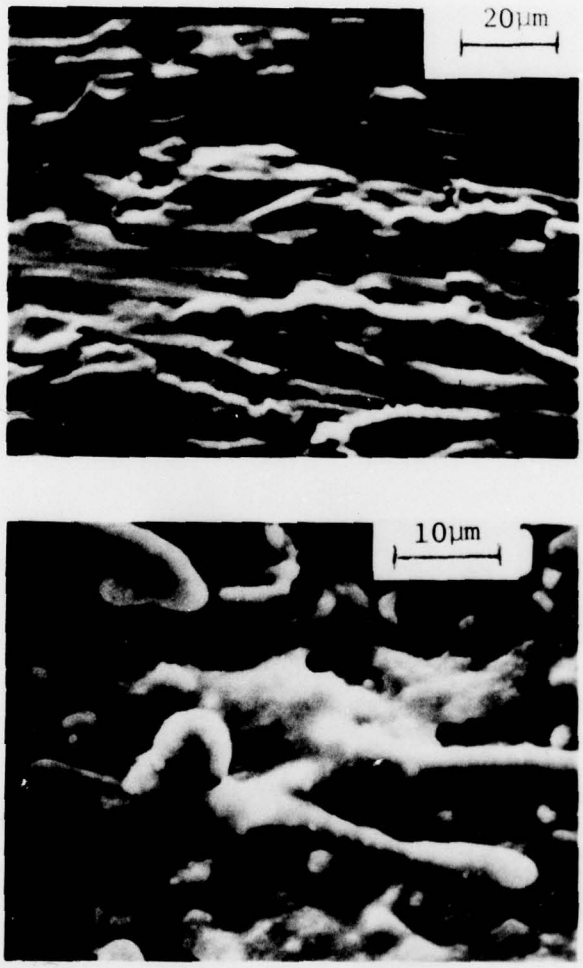

Fig. 33. Surface morphology on eroded aluminum alloy chips. (Christman, 1977).

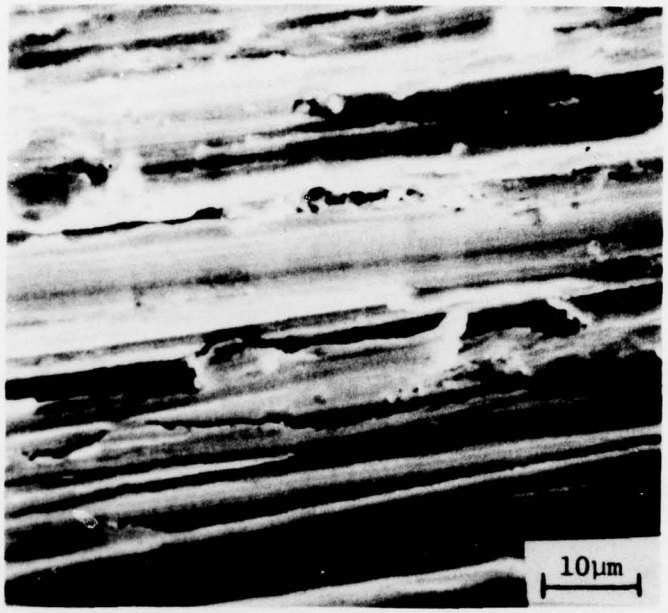

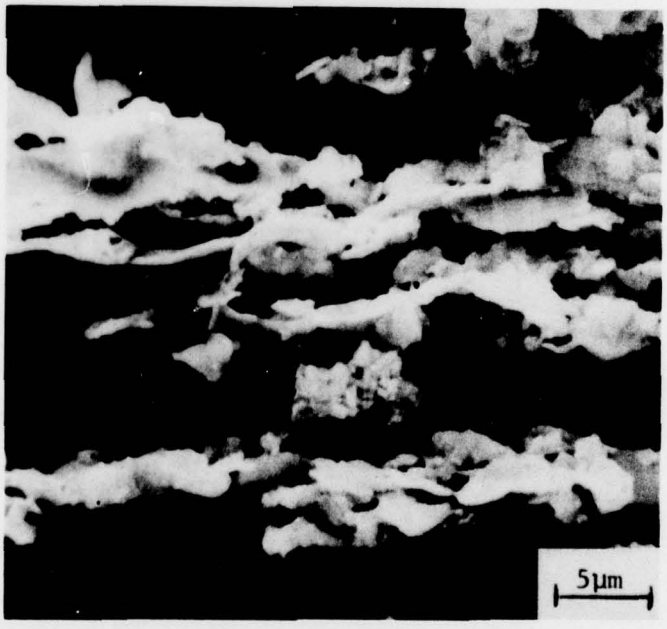

Fig. 34. Scanning electron micrographs of (a) the surface of abraded 1015 steel and (b) steel debris particles recovered after wear under dry conditions at 2.2 N load. (Ruff, 1978).

NBS-114A (REV. 7-73)

U.S. DEPT. OF COMM. BIBLIOGRAPHIC DATA SHEET	1. PUBLICATION OR REPORT NO. 78-1575	2. Gov't Accession No.	3. Recipient's Accession No.

4. TITLE AND SUBTITLE

(6) Erosion by Solid Particle Impact,

5. Publication Date

(11) January 1979

6. Performing Organization Code

7. AUTHOR(S)

(10) A. W. Ruff and S. M. Wiederhorn

8. Performing Organ. Report No.

9. PERFORMING ORGANIZATION NAME AND ADDRESS

NATIONAL BUREAU OF STANDARDS
DEPARTMENT OF COMMERCE
WASHINGTON, D.C. 20234

10. Project/Task/Work Unit No.

5640134

11. Contract/Grant No.

(12) 105p.

12. Sponsoring Organization Name and Complete Address (Street, City, State, ZIP)

(9) Interim rept.,

13. Type of Report & Period Covered

14. Sponsoring Agency Code

15. SUPPLEMENTARY NOTES

(14) NBSIR-78-1575

16. ABSTRACT (A 200-word or less factual summary of most significant information. If document includes a significant bibliography or literature survey, mention it here.)

A review of the methods and findings associated with solid particle impact erosion of metals and ceramics is presented. Modern theories of particle erosion and critically reviewed experimental observations are brought together and compared. Conclusions regarding the present state of understanding of erosion are given.

17. KEY WORDS (six to twelve entries; alphabetical order; capitalize only the first letter of the first key word unless a proper name; separated by semicolons)

Abrasives; ceramics; erosion; impact; metals; particle erosion; wear.

18. AVAILABILITY

[XX] Unlimited

[ ] For Official Distribution. Do Not Release to NTIS

[ ] Order From Sup. of Doc., U.S. Government Printing Office Washington, D.C. 20402, SD Cat. No. C13

[X] Order From National Technical Information Service (NTIS) Springfield, Virginia 22151

19. SECURITY CLASS (THIS REPORT)	21. NO. OF PAGES
UNCLASSIFIED	104
20. SECURITY CLASS (THIS PAGE)	**22. Price**
UNCLASSIFIED	$6.50

USCOMM-DC 29042-P74

411036

JOB